







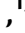







# A *Ralstonia solanacearum* effector targets TGA transcription factors to subvert salicylic acid signaling

Peipei Qi <sup>1,2,‡</sup> Mengling Huang <sup>1,2,‡</sup> Xuehan Hu <sup>1,2,‡</sup> Ying Zhang <sup>1,2</sup> Ying Wang <sup>1,2</sup>  
Pengyue Li <sup>1,2</sup> Shiyun Chen <sup>1,2</sup> Dan Zhang <sup>1,2</sup> Sen Cao <sup>1,2</sup> Wanting Zhu <sup>1,2</sup> Jiatao Xie <sup>1,2</sup>  
Jiasen Cheng <sup>1,2</sup> Yanping Fu <sup>1,2</sup> Daohong Jiang <sup>1,2</sup> Xiao Yu <sup>1,2</sup> and Bo Li <sup>1,2,\*†</sup>

1 State Key Laboratory of Agricultural Microbiology, Hubei Hongshan Laboratory Wuhan, Hubei, China

2 Hubei Key Lab of Plant Pathology, College of Plant Science and Technology, Huazhong Agricultural University, Wuhan, Hubei, China

\*Author for correspondence: boli@mail.hzau.edu.cn

†Senior author.

‡These authors contributed equally (P.Q., M.H., X.H.).

P.Q., M.H., X.H., and B.L. conceived the project, designed experiments, and analyzed the data. P.Q., M.H., X.H., Y.W., P.L., S.C., D.Z., and W.Z. performed experiments and analyzed the data. Y. Z. analyzed the RNA-seq data. J.X., Y.F., J.C., D.J., and X.Y. analyzed the data, provided critical feedback, and helped shape the research. X.Y. and B.L. wrote the manuscript with input from all co-authors.

The author responsible for distribution of materials integral to the findings presented in this article in accordance with the policy described in the Instructions for Authors (<https://academic.oup.com/plcell>) is: Bo Li (boli@mail.hzau.edu.cn).

## Abstract

The bacterial pathogen *Ralstonia solanacearum* causes wilt disease on *Arabidopsis thaliana* and tomato (*Solanum lycopersicum*). This pathogen uses type III effectors to inhibit the plant immune system; however, how individual effectors interfere with plant immune responses, including transcriptional reprogramming, remain elusive. Here, we show that the type III effector RipAB targets Arabidopsis TGACG SEQUENCE-SPECIFIC BINDING PROTEIN (TGA) transcription factors, the central regulators of plant immune gene regulation, via physical interaction in the nucleus to dampen immune responses. RipAB was required for *R. solanacearum* virulence on wild-type tomato and Arabidopsis but not Arabidopsis *tga1 tga4* and *tga2 tga5 tga6* mutants. Stable expression of RipAB in Arabidopsis suppressed the pathogen-associated molecular pattern-triggered reactive oxygen species (ROS) burst and immune gene induction as well as salicylic acid (SA) regulons including *RBOHD* and *RBOHF*, responsible for ROS production, all of which were phenocopied by the *tga1 tga4* and *tga2 tga5 tga6* mutants. We found that TGAs directly activate *RBOHD* and *RBOHF* expression and that RipAB inhibits this through interfering with the recruitment of RNA polymerase II. These results suggest that TGAs are the *bona fide* and major virulence targets of RipAB, which disrupts SA signaling by inhibiting TGA activity to achieve successful infection.

## Introduction

Bacterial wilt caused by the destructive soil-borne pathogen *Ralstonia solanacearum* leads to great economic losses worldwide every year (Peeters et al., 2013a). The *R. solanacearum* species complex has a wide host range including many important crops and vegetables, such as members of the *Solanaceae* family (Mansfield et al., 2012), and the model plant *Arabidopsis thaliana*. This pathogen invades from the

root and occupies stem xylem vessels, then quickly spreads to the aerial parts, eventual resulting in plant wilt and death. Various factors contribute to *R. solanacearum* infection and virulence (Genin and Denny, 2012). Cell wall degradation enzymes, exopolysaccharide, type III effectors (T3Es), and bacterial motility are necessary for its colonization and occupation of the xylem vessels, resulting in vascular dysfunction

that causes wilt symptoms. During infection, the expression of bacterial pathogenicity-related genes are controlled by a sophisticated network, including PHENOTYPE CONVERSION A (PhcA), which is a LysR-type transcription factor (Genin and Denny, 2012).

Plants have evolved robust innate immunity to fend off potential pathogens. Cell membrane- and cytosolic-localized receptor proteins monitor the invasion and activities of microbial pathogens (Zhou and Zhang, 2020). The *R. solanacearum*-related pathogen-associated molecular pattern (PAMP) elongation factor peptide elf18 is recognized by the pattern recognition receptor (PRR) ELONGATION FACTOR RECEPTOR (EFR) in Arabidopsis in *Brassicaceae* family (Kunze et al., 2004). CSP22 peptide from cold shock protein is detected by plants within *Solanaceae* family (Wei et al., 2018). Interestingly, the sequence of *R. solanacearum* flagellin protein underwent mutation during evolution, likely to avoid the *Solanaceae* host recognition, but could be recognized by GmFLAGELLIN-SENSING2 from the nonhost plant soybean (*Glycine max*; Wei et al., 2020). Pattern-triggered immunity (PTI) signaling activates downstream typical immune responses including  $\text{Ca}^{2+}$  influx, reactive oxygen species (ROS) burst, MITOGEN-ACTIVATED PROTEIN KINASE (MAPK) activation and transcriptional reprogramming (Yu et al., 2017). Immune genes related to signaling transduction, hormone biosynthesis, kinase activity, and antimicrobial compounds are rapidly induced post PAMP perception (Lewis et al., 2015). Coordination of the diverse transcription factors, epigenetic modification-related factors, and RNA polymerase II (Pol II) orchestrates immune gene expression (Li et al., 2016).

The plant defense-related hormones salicylic acid (SA), jasmonic acid (JA), and ethylene are induced to synthesize and play significant roles in both local and systemic resistance (Pieterse et al., 2009). These signaling molecules activate specific downstream pathway and thousands of gene expression, which consist of the important branches of resistance (Hillmer et al., 2017). SA is also known to potentiate the flg22-induced ROS burst, which is completely dependent on RESPIRATORY BURST OXIDASE PROTEIN D (RBOHD) (Sato et al., 2010; Xu et al., 2014). However, the mechanism by which SA potentiates the ROS burst remains elusive.

Arabidopsis NONEXPRESSOR OF PATHOGENESIS-RELATED 1 (NPR1), NPR3, and NPR4 are required for SA-mediated responses, in which they bind SA and function as the SA receptors (Cao et al., 1994; Wang et al., 2020). Intriguingly, NPR1 and NPR3/4 play positive and negative roles in transcriptional regulation of SA-related immune gene expression, respectively (Ding et al., 2018). When the SA level is low in the uninfected state, NPR3/4 interact with TGACG SEQUENCE-SPECIFIC BINDING PROTEIN 2 (TGA2)/TGA5/TGA6 and function as transcriptional suppressors. When the SA level increases during infection, the transcription repression function of NPR3/4 is released; meanwhile, NPR1 recruits TGA2/TGA5/TGA6 to activate downstream gene expression (Ding et al., 2018). Histone acetyltransferases

(HACs) exist in a complex and positively regulate SA-responsive gene expression (Jin et al., 2018). More than two thousand genes are differentially expressed in response to SA treatment, and the defense-related genes are enriched in the upregulated subgroup (Ding et al., 2018).

TGA transcription factors belong to the plant basic leucine zipper protein (bZIP) transcription factor superfamily, and *A. thaliana* has 10 members of the TGA family. Among them, seven TGAs are involved in defense, including clade I members TGA1 and TGA4, clade II members TGA2, TGA5, and TGA6, and clade III members TGA3 and TGA7 (Gatz, 2013). In particular, TGA2, TGA5, and TGA6 have been implicated in the activation of SA-responsive genes, including PATHOGENESIS-RELATED1 (*PR1*; Zhang et al., 2003). The *tga2 tga5 tga6* (*tga2/5/6*) triple mutant completely lost SA-induced resistance and is hypersensitive to SA, resembling the *npr1* mutant. The *PR1* promoter contains sequences, which are the direct binding sites of TGA2/5/6 (Zhang et al., 1999). TGA1 and TGA4 display weak or no detectable interaction with NPR1, suggesting their function is independent of NPR1 (Zhou et al., 2000). They regulate pipecolic acid and SA biosynthesis by modulating the expression of SAR DEFICIENT 1 (*SARD1*) and CAM-BINDING PROTEIN 60-LIKE G (*CBP60g*) in plant basal defense (Sun et al., 2018). Thus, TGA transcription factors serve as central hub regulators of plant immunity.

Pathogens often target central regulators of plant immunity. For example, *Pseudomonas syringae* type III effector AvrPtoB directly targets NPR1 and promotes ubiquitination-mediated NPR1 degradation (Chen et al., 2017). This makes sense, as targeting immunity hubs can dampen a large part of immune responses that are regulated by the hub. Thus, whether pathogen effectors directly target TGA transcription factors is an important question to be addressed.

Similar to with other phyto-bacterial pathogens, the main determinant of *R. solanacearum* pathogenicity is the type III secretion system (T3SS). The *R. solanacearum* *hrcC* mutant, which is defective in a key component of the T3SS, completely lost virulence (Genin and Denny, 2012). *Ralstonia solanacearum* encodes more type III effectors than other bacterial pathogens, with more than 110 T3Es predicted in the pangenome of *R. solanacearum* sequenced strains with an average of approximately 70 effectors in one strain (Peeters et al., 2013b). However, only a handful of *R. solanacearum* effectors were demonstrated to function during infection (Deslandes and Genin, 2014). The GALA family effectors, which are F-box containing proteins, interfere with the host ubiquitin/proteasome pathway to promote disease (Angot et al., 2006). RipAY is activated by plant thioredoxins and suppresses host immunity by degrading glutathione (Mukaihara et al., 2016). Plant chloroplast-localized T3E RipAL induces JA production to suppress SA-induced defenses. RipI and the TALE-like effector Brg11 manipulate plant metabolism to promote infection and compete with other microbes (Wu et al., 2019; Xian et al., 2020). Plant nucleus-localized T3Es interfere with plant immunity by

modulating gene expression. For example, PopP2 acetylates several WRKY transcription factors (Le Roux et al., 2015; Sarris et al., 2015). While these studies revealed how some *R. solanacearum* T3Es manipulate plant immune responses for successful infection, we still lack the comprehensive knowledge required for development of effective, sustainable solutions to plant disease caused by this devastating pathogen.

In this study, we show the molecular basis of the T3E RipAB for virulence. By phenotypic characterization of *R. solanacearum* mutants and transgenic and mutant plants, we demonstrate that TGAs are the bona fide and major virulence targets of RipAB. We show that RipAB disrupts SA signaling by interfering with the ability of TGAs to recruit RNA Pol II at their regulons. This study advances our understanding of plant immune signaling networks and the virulence mechanism of *R. solanacearum*, which could help researchers to develop solutions to plant disease caused by this devastating pathogen.

## Results

### RipAB suppresses plant immune responses

To identify *R. solanacearum* effectors interfering with plant immune gene expression, we screened 8 plant nuclear localized Type III effectors from *R. solanacearum* strain GMI1000 (Supplemental Figure S1A). The promoters of *FRK1* and *WRKY30*, two early PTI marker genes fused to a firefly luciferase (*LUC*) reporter gene, were strongly activated by elf18 treatment. The SA analog 2,6-dichloroisonicotinic acid (INA) activated *PR1* expression, which is a marker for SA signaling. Among the effectors we screened, RipAB dramatically suppressed elf18-induced activation of *FRK1* and *WRKY30*, and INA-activated *PR1* expression in Arabidopsis protoplasts (Figure 1A; Supplemental Figure S1, B and C and Supplemental Figure S2A). Interestingly, when we transiently expressed RipAB in *Nicotiana benthamiana*, the ROS burst induced by flg22 was greatly inhibited compared with that expressing empty *GREEN FLUORESCENT PROTEIN* (*GFP*) control (Figure 1B). However, the overexpression of RipAB did not affect elf18-triggered MAPK activation in Arabidopsis protoplasts (Supplemental Figure S2B). These results indicated that RipAB may target specific branches of plant immunity such as SA and ROS.

RipAB encodes a 174-amino acid (aa) protein containing a potential bipartite nuclear localization signal (Bi-NLS) spanning the 96–118 aa with two interdependent basic clusters separated by a 13-aa linker. There is no known functional domain within the sequence. When expressed in Arabidopsis protoplasts, RipAB is specifically localized in the nucleus (Supplemental Figure S2C), further suggesting its function in modulating host gene expression. To investigate whether the nuclear localization is required for RipAB to suppress plant immune gene expression, we mutated K93–K96 to Alanine (RipAB<sup>4KA</sup>), K113–R118 to Alanine (RipAB<sup>5KA</sup>), or both the NLS clusters (RipAB<sup>nls</sup>) through site-directed mutagenesis. When transiently expressed in Arabidopsis protoplasts, the mutated variants exhibited higher molecular weight than the

wild-type (WT) protein, likely due to the loss of positive charges of amino acids (Supplemental Figure S2D). Individual mutation of either NLS cluster partially blocked the nuclear localization, and the RipAB<sup>nls</sup> mutant lost most of the nuclear localization compared with WT RipAB (Figure 1C; Supplemental Figure S2E). RipAB<sup>4KA</sup> and RipAB<sup>5KA</sup> could still suppress elf18-induced *FRK1* and INA-induced *PR1* expression but RipAB<sup>nls</sup> significantly lost the ability to inhibit *FRK1* and *PR1* induction (Figure 1D). In concert, RipAB<sup>nls</sup> was unable to suppress the flg22-induced ROS burst in *N. benthamiana* compared to the WT RipAB (Figure 1E). Taken together, these results suggest that RipAB localizes in the nucleus, and this nuclear localization is required for it to suppress plant immune responses.

### RipAB plays an important role in plant and bacteria interaction

To further study the inhibitory impact of RipAB on plant immunity, stable Arabidopsis transgenic plants constitutively expressing RipAB driven by the CaMV 35S promoter were generated in the WT Col-0 background. Two independent lines, OE-1 and OE-21, with similar RipAB expression levels were chosen for further assays (Supplemental Figure S3A and S3B). Compared to the WT, the RipAB overexpression plants were slightly smaller, and with longer petioles (Supplemental Figure S3A). The nuclear localization of RipAB was also confirmed in the transgenic lines (Supplemental Figure S2F).

We further characterized these RipAB overexpression plants for plant immune responses. In line with the protoplast reporter assay, the immune marker genes *FRK1*, *WRKY30*, and *NHL10* showed lower induction upon elf18 treatment in RipAB overexpression lines than WT (Figure 1F). In addition, INA-induced *PR1* and *WRKY70* expression was lower in RipAB overexpression lines (Figure 1G). Consistent with the results from the *N. benthamiana* transient assay, we found flg22-triggered ROS production was reduced to 60% of WT levels, while elf18-induced MAPK activation remained WT-like in RipAB overexpression lines (Figure 1, H and I). Previous studies showed that SA pretreatment enhanced flg22-induced callose deposition and SA signaling regulated the expression of callose synthase genes (Dong et al., 2008; Tateda et al., 2014). Interestingly, we found that elf18-induced callose deposition, another hallmark of plant immunity, was about 80% lower in overexpression lines than in WT plants (Figure 1J). Thus, the presence of RipAB interferes with specific branches of plant innate immunity.

Next, we investigated whether RipAB influences plant resistance against infection by *R. solanacearum* GMI1000. RipAB overexpression lines displayed more severe and faster disease symptoms compared with WT plants (Figure 2, A and B). Bacterial titers in the RipAB overexpression lines were 8- to 10-fold higher than that in the WT plants at 6-day post inoculation, indicating that RipAB expression could impair plant resistance against *R. solanacearum* (Figure 2C). In contrast, RipAB<sup>nls</sup> overexpression plants were as



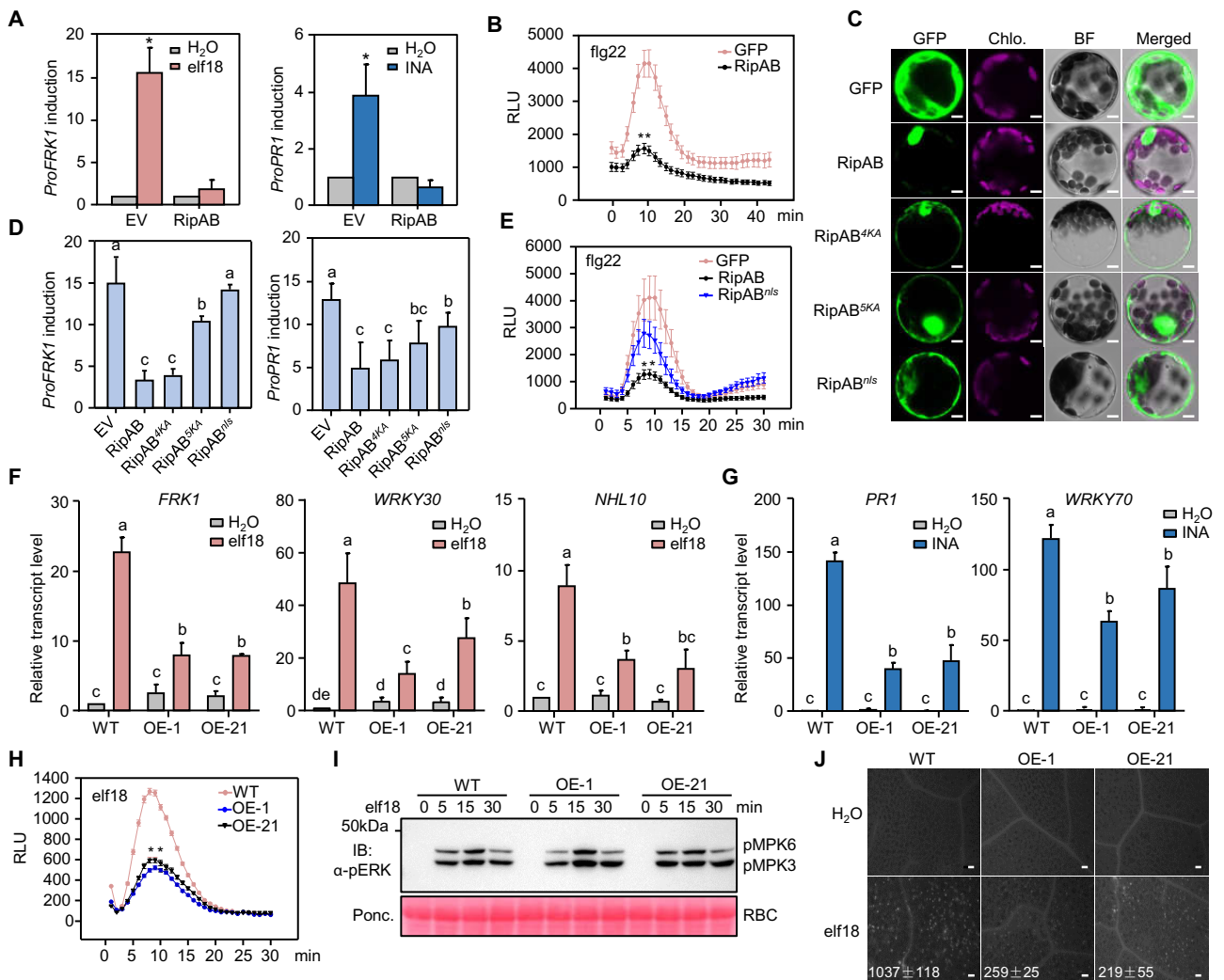


**Figure 1** RipAB suppresses plant immune responses. **A**, RipAB suppresses elf18-induced *FRK1* expression and INA-induced *PR1* expression in Arabidopsis. *pFRK1::LUC* or *pPR1::LUC* were co-transfected with *RipAB* or an empty vector control in protoplasts and treated with 100-nM elf18 or 100- $\mu$ M INA. Error bars represent  $\pm$  SD of three biological replicates. **B**, RipAB inhibits flg22-induced ROS burst in *N. benthamiana*. Leaf discs expressing RipAB or GFP were treated with 100-nM flg22, and the relative light units were detected. Values represent means  $\pm$  SE ( $n = 15$ ). **C**, RipAB is localized in the nucleus of Arabidopsis. Protoplasts were transfected with *RipAB-GFP*, the nuclear localization mutants or *GFP* control. Chlo. indicates chloroplasts and BF means bright field. Scale bars indicate 10  $\mu$ m. **D**, RipAB nuclear localization is required for suppressing *FRK1* and *PR1* induction. Values represent means  $\pm$  SD ( $n = 3$  biological replicates). **E**, RipAB nuclear localization is required for inhibiting ROS burst. Leaf discs expressing *RipAB-GFP*, *RipAB<sup>nls</sup>-GFP*, or *GFP* control were treated with 100-nM flg22. Values represent means  $\pm$  SE ( $n = 15$  biological replicates). **F**, Compromised early immune-related gene induction in RipAB overexpression lines. Seedlings were treated with or without 100-nM elf18 for 1 h. Data were normalized to the expression of *ACTIN2* in RT-qPCR analysis. **G**, Compromised INA-induced *PR1* and *WRKY70* expression in RipAB overexpression lines. **H**, elf18-induced ROS burst is suppressed in RipAB overexpression lines. Leaf discs from 4-week-old plants were treated with 100-nM elf18 and values represent means  $\pm$  SE ( $n = 15$  biological replicates). **I**, Overexpression of RipAB does not affect elf18-induced MAPK activation. MAPK activation was detected by immunoblotting with an  $\alpha$ -pERK antibody (top). Protein loading was shown by Ponceau S staining for RBC (bottom). **J**, Compromised elf18-induced callose deposition in RipAB overexpression lines. Values represent means  $\pm$  SD ( $n = 5$  biological replicates). Scale bars indicate 10  $\mu$ m. The above experiments were repeated three times with similar results. Values in (F) and (G) represent means  $\pm$  SD of three technical replicates from one repeat. Asterisk indicates a significant difference (Student's one-tailed *t* test, \* $P < 0.05$ , \*\* $P < 0.01$ ) when compared with control. Different letters are used to indicate samples with significant differences (one-way ANOVA,  $P < 0.05$ ).

susceptible as the WT (Figure 2D; Supplemental Figure S3, C and E). In addition, elf18-triggered ROS production in *RipAB<sup>nls</sup>* overexpression plants was similar to WT levels (Supplemental Figure S3F). These results are consistent with the previous result showing that *RipAB<sup>nls</sup>* was unable to suppress immune gene induction (Figure 1D).

To determine whether RipAB is critical for *R. solanacearum* pathogenicity, we deleted *RipAB* in GMI1000 background through homologous recombination. Two independent *RipAB* deletion strains were identified (Supplemental Figure S3G). Furthermore, the complementation strains with native promoter-driven *RipAB-HA* were

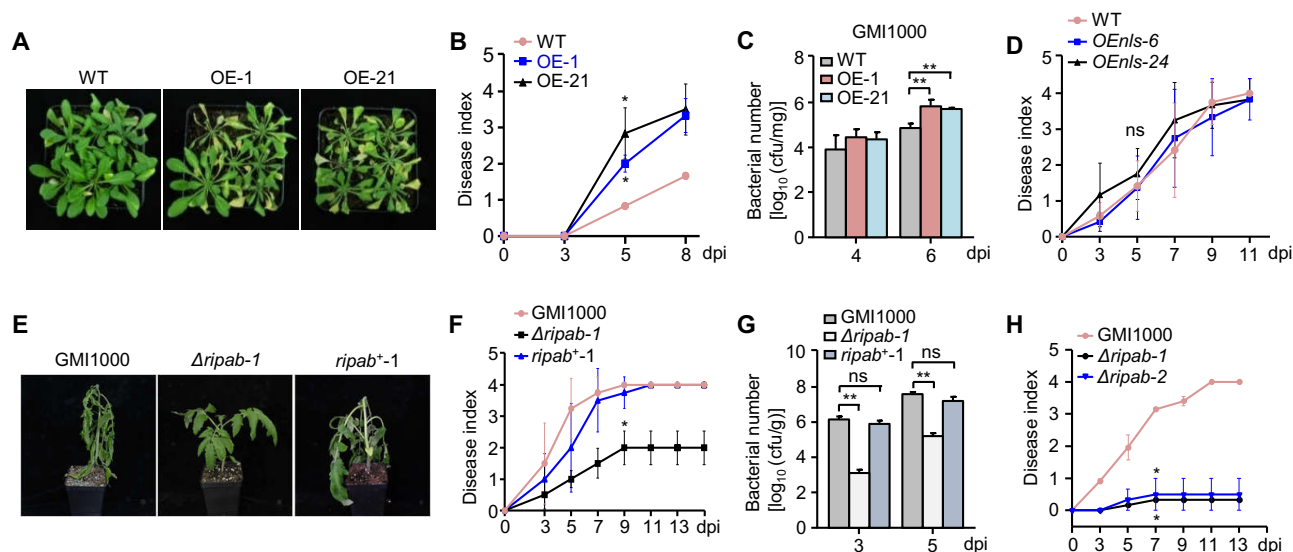


**Figure 2** RipAB is required for *R. solanacearum* virulence. A–C, Compromised resistance to *R. solanacearum* in RipAB overexpression lines. Soil-drenching inoculation assay were performed with GMI1000 on WT and RipAB overexpression plants. Plant symptom pictures (A) were taken at 7 dpi, disease index of plant symptom (B) was quantified at depicted time points from 12 biological repeats, bacterial growth of inoculated Arabidopsis roots (C) was quantified at 4 and 6 dpi from three biological repeats. D, Disease index of WT and RipAB<sup>nlis</sup> overexpression lines upon GMI1000 inoculation were quantified at depicted time points ( $n = 6$  biological repeats). E–G, Compromised virulence of  $\Delta ripab$  mutant to tomato accession Money Maker. Soil-drenching inoculation assay was performed with GMI1000,  $\Delta ripab$  mutant, and RipAB complementation strain ( $ripab^+$ ) on 4-week-old tomato plants. Pictures of disease symptoms were taken at 5 dpi (E). Disease index of plant symptom (F) and bacterial growth number of tomato roots (G) were quantified at 3 and 5 dpi from six biological repeats. H, Two  $\Delta ripab$  mutant strains show compromised pathogenicity to Arabidopsis. Soil drenching inoculation assay were performed in Arabidopsis WT plants. Disease indexes were quantified at the depicted time points from six biological repeats. Values represents means  $\pm$  SD and asterisk indicates a significant difference with control (Student's one-tailed  $t$  test, \* $P < 0.05$ , \*\* $P < 0.01$ ).

enerated in the  $\Delta ripab-1$  knockout mutant background. Interestingly, the RipAB-AB fusion protein could not be detected in the complementation strain grown in media, but was expressed when the complementation strain was grown in tomato roots (Supplemental Figure S3, H and I). We tested the *R. solanacearum* WT,  $\Delta ripab-1$  knockout, and complementation strains in the tomato accession Money Maker. The  $\Delta ripab$  strains caused a very weak wilting phenotype or even completely lost pathogenicity (Figure 2, E and F), and bacterial titers in tomato stem were 1,000 times lower than WT strain (Figure 2G). Importantly, the complementation strain showed restored virulence, and the bacterial titers were comparable with the WT strain during infection (Figure 2, E and H). We also inoculated Arabidopsis plants with GMI1000 and the  $\Delta ripab$  strains. Similarly, neither of these  $\Delta ripab$  strains could infect Arabidopsis and cause wilt phenotype 10 days after inoculation (Figure 2H). The bacteria titer of  $\Delta ripab$  strains in Arabidopsis roots was lower than the WT GMI1000 (Supplemental Figure S3J). To exclude the possibility that the reduced virulence and multiplication in plants were due to the compromised growth of  $\Delta ripab$ , we monitored the growth of WT and mutant strains. Both strains showed similar growth rate in the medium (Supplemental Figure S3K). These data indicate that RipAB is required for *R. solanacearum* GMI1000 virulence in both tomato and Arabidopsis.

### RipAB interacts with members of the TGA transcription factor family

We then sought for RipAB target proteins in plants. To this end, RipAB-GFP was transiently expressed in *N. benthamiana* leaves and in planta co-immunoprecipitation (Co-IP) was performed with anti-GFP Trap followed by liquid chromatography–mass spectrometry/mass spectrometry (LC–MS/MS). The GFP protein was expressed and used as a control to exclude nonspecific binding. Twenty-four plant nuclear-localized proteins were identified in total (Supplemental Data Set S1). Based on the observation that RipAB interferes with immune gene expression, a transcription factor, TGA2, was selected for further study due to its well characterized role in SA signaling (Zhang et al., 2003). TGA transcription factors belong to the basic leucine zipper transcription factors family and *A. thaliana* contains ten members of the TGA family (Supplemental Figure S4A). Among these Arabidopsis TGA proteins, clade I consists of TGA1 and TGA4; clade II consists of TGA2, TGA5, and TGA6; and clade III consists of TGA3 and TGA7; moreover, Arabidopsis TGAs have been reported to play critical roles in plant immunity (Zhang et al., 2003; Droge-Laser et al., 2018).

To confirm RipAB interaction with TGA2 as well as with other immunity-related TGAs, we performed bimolecular fluorescence complementation (BiFC) assays in *N. benthamiana* leaves. Nuclear localized ARABIDOPSIS SH4-RELATED 3 (ASR3), an immune-related transcription factor, was fused

with cYFP and included as a negative control (Li et al., 2015). The BiFC showed that RipAB associated with TGA1, TGA2, TGA3, TGA4, TGA5, and TGA6 in the nucleus. However, no YELLOW FLUORESCENT PROTEIN (YFP) signal was observed for TGA7 and ASR3 (Figure 3A).

We also performed split-LUC assay to investigate the association of RipAB with TGAs and observed that when co-expressed with RipAB-nLUC in *N. benthamiana* leaves, all TGAs (TGA1–TGA7) fused with C-terminal LUC showed strong LUC signals with different strength (Figure 3B). This result was supported by the quantification of relative LUC activity (Supplemental Figure S4B). These results were further confirmed by Co-IP assay in Arabidopsis protoplasts showing that FLAG-tagged TGA1–TGA7 could co-immunoprecipitated with HA-tagged RipAB (Figure 3C). In concert, HEMAGGLUTININ (HA)-tagged TGAs protein could be immunoprecipitated by RipAB-GFP (Figure 3D). Thus, RipAB associates with TGA1–TGA7 in planta.

In order to determine whether RipAB directly or indirectly interacts with TGAs, we performed in vitro pull-down assay using purified GST-TGAs and MBP-RipAB fusion recombinant proteins. MBP-RipAB was pulled down by all tested GST-TGAs, pointing to their direct interactions (Figure 3E). Since the N-terminus of TGA contains a bZIP DNA binding domain and the C-terminus is required for interaction with NPR1 (Zhou et al., 2000), we also tested the interaction of the TGA2 N- and C-termini with RipAB. Similar to the full-length TGA2, both TGA2N and TGA2C could be pulled down by MBP-RipAB (Supplemental Figure S4C). These data suggest that RipAB directly targets multiple clades of TGA transcription factors in plants.

### RipAB-overexpressing plants phenocopy *tga* mutants in plant immunity

We next tested whether TGA functions in plant immunity were affected by RipAB. TGA1 and TGA4 are required for plant basal defense and SA biosynthesis gene expression (Sun et al., 2018). In order to determine whether RipAB generally suppressed plant immune systems, we performed disease assays using foliar hemi-biotrophic pathogen *Pseudomonas syringae* pv. *tomato* (*Pst*) DC3000. Three days post bacterial infection, the leaves of RipAB overexpression plants showed more disease symptoms (yellowish color and water soaking), and supported more bacteria growth compared with the WT (Figure 4A; Supplemental Figure S5A). Consistent with the *tga1 tga4* mutant phenotype, the transgenic plants exhibited compromised flg22-induced disease resistance compared with the WT (Figure 4B; Supplemental Figure S5B).

*SARD1* and *CBP60g* were identified as target genes of TGA1 and TGA4 in basal defense, which further regulates SA signaling pathway (Sun et al., 2018). We found that *P. syringae* pv. *maculicola* (*Psm*) ES4326 infection induced *SARD1* and *CBP60g* expression, which were less induced in both *tga1 tga4* mutants and RipAB overexpression lines (Figure 4C). In addition, *Psm* infection-activated *PR1* and *WRKY70* expression were suppressed by the presence of

RipAB (Supplemental Figure S5C). Therefore, the data suggested that the expression of RipAB in planta inhibits TGA1/TGA4-mediated plant immunity.

A previous study showed that the *tga2 tga5 tga6* triple mutant (*tga2/5/6*) is hypersensitive to SA (Zhang et al., 2003). We found that two RipAB overexpression lines were hypersensitive to the SA analog INA, similar to *tga2/5/6* mutants (Figure 4D). SA-induced resistance and systemic-acquired resistance (SAR) are compromised in *npr1* and *tga2/5/6* mutants (Cao et al., 1997; Zhang et al., 2003). We tested whether RipAB influences INA-induced resistance. *Pst* DC3000 grew 10-fold less in INA-pretreated leaves than in water-treated leaves in the WT. However, two RipAB overexpression lines did not display INA-induced resistance (Figure 4E). We also measured SAR activated by pre-inoculation of the lower leaves with *Pst avrRpt2* followed by the inoculation of upper leaves with *Pst* DC3000. WT plants showed strong resistance to the secondary infection; however, *tga2/5/6* and RipAB overexpression plants almost completely lost SAR (Figure 4F). These data suggest that the overexpression of RipAB in Arabidopsis could block TGA2/TGA5/TGA6-related plant immunity.

To elucidate the biological relevance of TGAs in RipAB virulence function, we challenged *tga1/4* and *tga2/5/6* mutants with GMI1000 and  $\Delta$ *ripab* mutant strain. The *tga1/4* mutant showed faster disease development and higher *R. solanacearum* titer compared with WT plants (Figure 4, G and H), indicating the important role of TGA1 and TGA4 in positively regulating resistance against *R. solanacearum*. The *tga2/5/6* mutants did not show a clear difference with WT upon GMI1000 infection. Importantly, in contrast to the significantly weak virulence to WT plants, the  $\Delta$ *ripab* mutant caused dramatically more severe and faster disease symptoms and accumulated higher bacterial titers in *tga2/5/6* mutant plants (Figure 4, G and H). We also observed mildly enhanced susceptibility of *tga1/4* upon  $\Delta$ *ripab* infection, and the bacterial titer of  $\Delta$ *ripab* was increased in *tga1/4* compared with in WT plants (Figure 4, G and H). Further, the presence of RipAB greatly inhibited elf18-induced *FRK1* and *WRKY30* expression in the WT (Supplemental Figure S5D). Similarly, INA-induced *PR1* and *WRKY70* expression was suppressed by RipAB in the WT (Figure 4). However, elf18 and INA barely induced marker gene expression in *tga1/4* and *tga2/5/6* mutants, respectively, and we could not detect a further effect of RipAB. These results indicate that TGAs are the *bona fide* targets of RipAB.

Since RipAB suppresses plant PTI responses and TGAs are the direct targets of RipAB, we therefore tested the involvement of TGAs in PTI. Consistent with the phenotype of RipAB overexpression plants, *tga1/4* and *tga2/5/6* mutants displayed compromised elf18-induced expression of early immune marker genes (Supplemental Figure S6A). In addition, the impaired INA-induced *PR1* and *WRKY70* expression was confirmed in *tga1/4* mutants (Supplemental Figure S6B). The elf18-induced ROS burst was largely compromised in both *tga1/4* and *tga2/5/6* mutants (Figure 4). In addition, *tga1/4* showed a greatly reduced ROS burst triggered by the



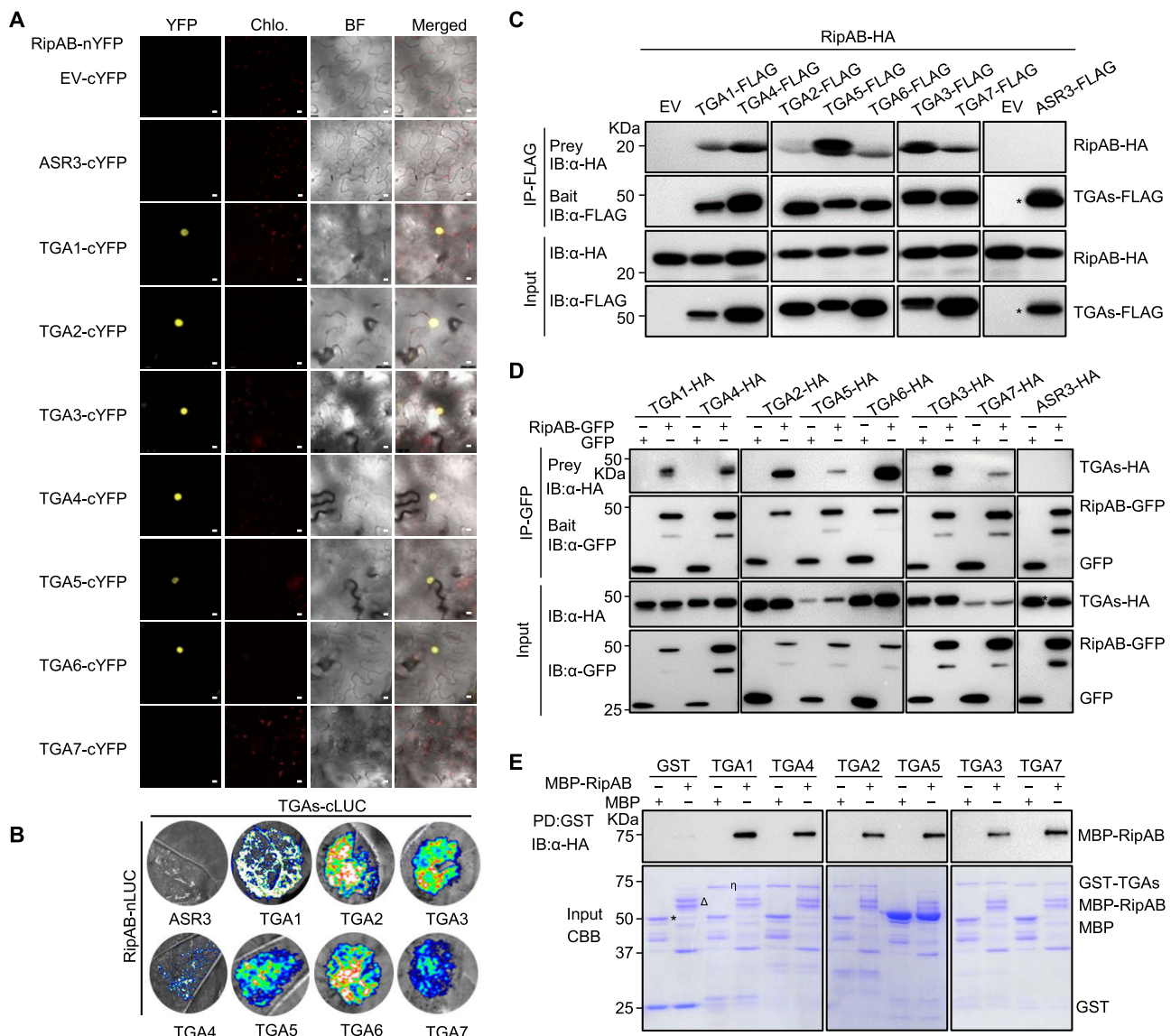


**Figure 3** RipAB interacts with TGA transcription factor family members. **A**, Interaction between RipAB and TGAs by BiFC assay. RipAB-nYFP and individual TGAs-cYFP were expressed in *N. benthamiana* leaves. The fluorescence signals were observed using confocal microscope. EV represents the empty vector control. Scale bars indicate 10  $\mu$ m. **B**, Interaction between RipAB and TGAs in split-LUC assay. RipAB-nLUC was co-expressed with TGAs-cLUC in *N. benthamiana* leaves. The luminescence intensity was detected by imaging system within 5 min after the supplement of substrate luciferin. **C**, RipAB associates with TGA1–TGA7 in protoplasts by Co-IP assay. RipAB-HA was co-expressed with FLAG-tagged TGA1–TGA7 in Arabidopsis protoplasts. Total protein extracts were immunoprecipitated with  $\alpha$ -FLAG Agarose beads and immunoblotted using an  $\alpha$ -HA or  $\alpha$ -FLAG antibody. Protein inputs are shown with immunoblotting before immunoprecipitation (bottom two parts). **D**, RipAB associates with TGA1–TGA7 in protoplasts by reverse direction Co-IP assay. RipAB-GFP was co-expressed with HA-tagged TGA1–TGA7 in Arabidopsis protoplasts. Total protein extracts were immunoprecipitated with GFP-Trap beads and immunoblotted using an  $\alpha$ -HA or  $\alpha$ -GFP antibody. Protein inputs are shown with immunoblotting before immunoprecipitation (bottom two parts). **E**, RipAB interacts with TGAs in an in vitro pull-down assay. GST or GST-TGAs (1  $\mu$ g) proteins were immobilized on glutathione Sepharose beads and incubated with MBP or MBP-RipAB (5  $\mu$ g) proteins. The beads were washed and pelleted for immunoblot analysis with an  $\alpha$ -HA antibody. Coomassie blue staining of input proteins is shown on the bottom.

PAMPs chitin and flg22 (Supplemental Figure S6C). We also found that elf18-induced callose deposition was largely suppressed in *tga2/5/6* mutants (Supplemental Figure S6D). These results further support the idea that RipAB suppresses plant PTI and basal defense by targeting TGAs. Altogether, TGAs are important for plant resistance to bacterial wilt disease and PTI, and RipAB targets TGAs to globally attenuate plant immunity.

### SA-responsive genes are globally suppressed by RipAB

To gain further insights into the influence of RipAB on SA-mediated immune gene reprogramming, we used RNA-seq to monitor the global gene expression profile in WT and oxRipAB plants 1-h post INA treatment (Supplemental Data Set S2). The gene expression pattern exhibited high correlation between WT and RipAB OX-21 plants without

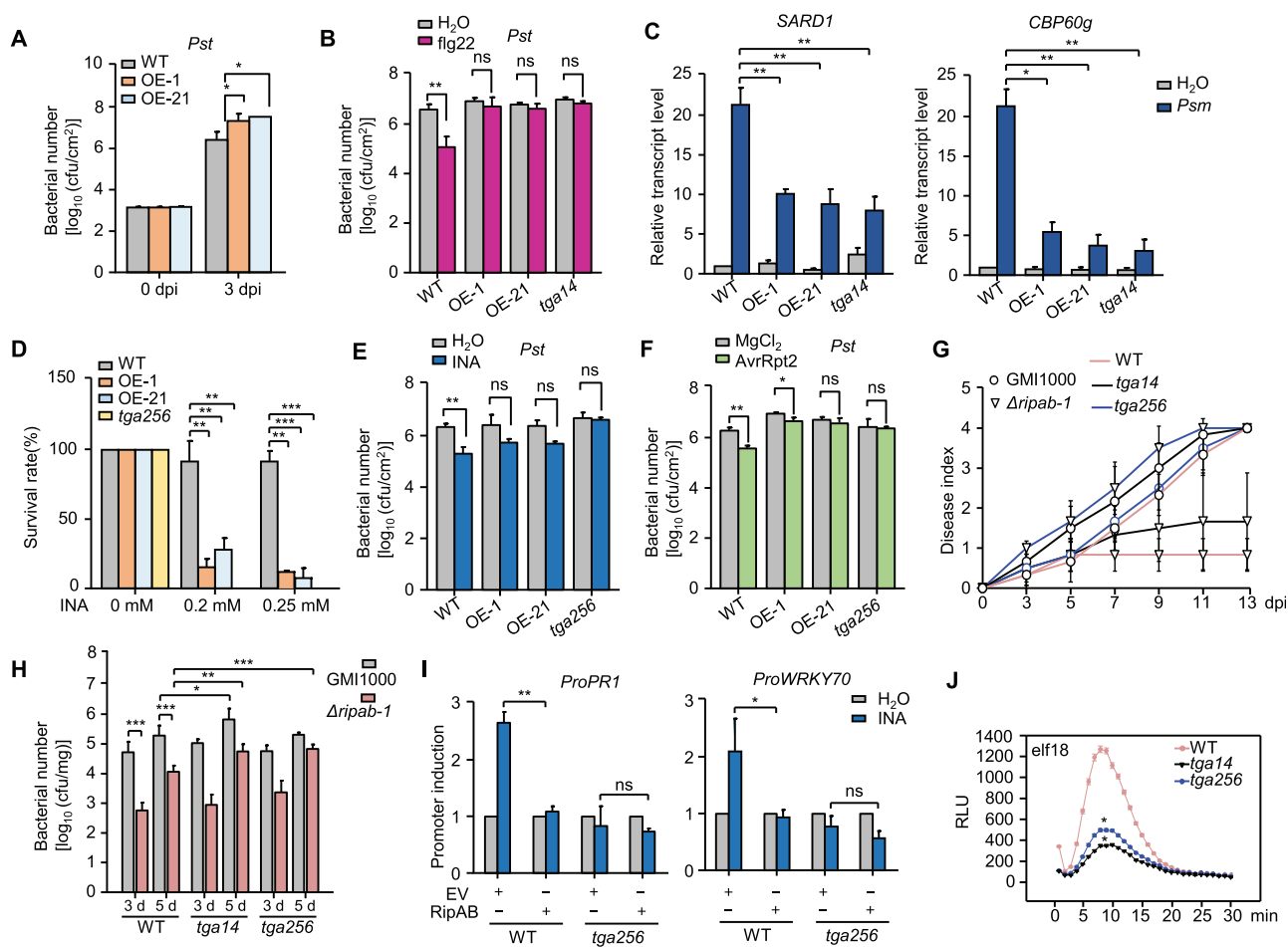


**Figure 4** RipAB overexpression plants phenocopy TGAs mutants in plant immunity. **A**, RipAB overexpression lines are more susceptible to *Pst* DC3000 than WT. Bacterial cell suspensions with  $OD_{600} = 5 \times 10^{-4}$  were infiltrated into leaves of 4-week-old plants. Bacterial populations were quantified at 0 and 3 dpi. **B**, RipAB overexpression lines exhibits compromised flg22-induced resistance to *Pst* DC3000. Plant leaves were infiltrated with *Pst* DC3000 24 h after ddH<sub>2</sub>O or flg22 pretreatment. Bacterial growth numbers were quantified at 3 dpi. **C**, RipAB overexpression lines suppress the *Psm* ES4326-induced *SARD1* and *CBP60g* similar as the *tga1 tga4* double mutant. Leaves of 4-week-old plants were infiltrated with bacterial suspensions at  $OD_{600} = 1 \times 10^{-3}$ . Samples were collected for RT-qPCR analysis at 12 hpi. Error bars are  $\pm$ SD of three technical replicates. **D**, RipAB overexpression lines are more sensitive to INA treatment. Plant seeds were germinated on MS medium supplemented with/without INA, survival rate of plants was quantified at the tenth day. The data are shown from 20 biological replicates. **E**, INA pretreatment induced weaker resistance to *Pst* DC3000 in RipAB overexpression lines. Plants were treated with 250- $\mu$ M INA before the infection of *Pst* DC3000. Bacterial growth numbers were quantified at 3 dpi. **F**, RipAB overexpression lines greatly lost the SAR. Depicted plants were infiltrated with MgCl<sub>2</sub> or avirulent *Pst* *avrRpt2* in lower leaves 3 days before the infiltration of *Pst* DC3000 at distal leaves. Bacterial populations were quantified at 3 dpi. **G**, **H**, The TGA factors are major virulent targets of RipAB. Soil-drenching inoculation assay was performed on WT and *tga* mutants with different bacterial strains, disease index (**G**) was scored at depicted time points (bars are means  $\pm$  SD,  $n = 12$  biological repeats) and bacterial growth number of Arabidopsis roots (**H**) were detected at 3 and 5 dpi (bars are means  $\pm$  SD,  $n = 5$  biological repeats). **I**, The inhibition of RipAB on INA-induced *PR1* and *WRKY70* expression is compromised in *tga2 tga5 tga6* mutants. *pPR1: LUC* or *pWRKY70: LUC* were co-transfected with *RipAB* or an empty vector control in protoplasts and the LUC activities were measured post-INA treatment ( $n = 3$  biological repeats). **J**, Elf18-induced ROS burst is suppressed in *tga1 tga4* and *tga2 tga5 tga6* mutants. Leave discs from WT and *tga* mutants were treated with 100-nM elf18 and the relative light units were detected ( $n = 15$  biological repeats). The above experiments were repeated three times with similar results. Bars in (**A**), (**B**), (**E**), and (**F**) represent means  $\pm$  SD (two leaflets each from  $n = 4$  independent plants). Asterisk indicates a significant difference (Student's one-tailed *t* test, \* $P < 0.05$ , \*\* $P < 0.01$ , \*\*\* $P < 0.001$ ) when compared with control.

treatment (Figure 5A), indicating the global gene expression did not change significantly upon RipAB overexpression. With the parameters of fold change  $\geq 2$  and  $q$ -value  $< 0.05$ , 1,165 upregulated genes and 342 downregulated genes by INA treatment for 1 h were identified in WT (Supplemental Data Sets S3 and S4). Notably, the INA-induced differentially expressed genes (DEGs) varied a lot between WT and

oxRipAB plants (Figure 5B). There were more up-regulated and downregulated genes in the WT than in oxRipAB plants (Figure 5C). The typical SA signaling-related genes and downstream target genes showed lower or no induction in oxRipAB plants (Figure 5D). In addition, callose biosynthesis-related genes were strongly upregulated in WT upon INA treatment but not in oxRipAB plants (Figure 5E), which



provides an explanation for the deposition of less callose induced by *elf18* in *oxRipAB* plants compared with WT (Figure 1J). These data are in line with the results that *oxRipAB* plants showed weaker immune defense upon INA treatment

Plant nucleus-localized RipAB obviously suppressed the PAMP-induced ROS burst and *tga* mutants are also compromised in ROS production. Therefore, we speculated that RipAB suppressed the expression of *RBOHD* and *RBOHF*, which encode the key enzymes on the cell membrane that generate PAMP-induced ROS. Indeed, the expression of *RBOHD* was induced more than seven-fold in WT upon INA treatment but not in *oxRipAB* plants (Figure 5F). The RNA-seq result was further verified by reverse transcription polymerase chain reaction (RT-qPCR), which showed that INA-induced *RBOHD* and *RBOHF* expression was much lower in *oxRipAB* than in WT plants (Figure 5G).

To test whether the suppression was related to TGA transcription factors, we determined the INA-induced *RBOH* expression in *tga1/4* and *tga2/5/6* mutants. Notably, the loss of TGA function largely attenuated *RBOHD* and *RBOHF* expression (Figure 5G). In addition, *elf18*-induced *RBOHD* and *RBOHF* expression was largely compromised in *oxRipAB* plants compared with WT (Figure 5H). Importantly, both *tga1/4* and *tga2/5/6* mutants also showed lower induction of *RBOHD* and *RBOHF* upon *elf18* treatment (Figure 5H). These results indicated that RipAB suppresses plant immune gene expression through interfering with TGA function and that the expression of *RBOHD* and *RBOHF* is dependent on TGA transcription factors.

### RipAB interferes with TGAs transcriptional activity

Since TGA factors are targets of RipAB, we investigated how RipAB influences TGA function. First, we tested the transcriptional activity of TGAs in the presence of RipAB with the GAL4 transcription system (Figure 6A). The INA-activated transcriptional activity of TGA2 and TGA6 were inhibited by co-expression of RipAB, as well as the *elf18*-induced transcriptional activity of TGA1 and TGA4 (Figure 6B). Thus, the effector RipAB interacts with TGAs and suppresses their transcriptional activity, thereby affecting the expression of downstream immune genes.

To further explore the mechanism by which RipAB affects the transcriptional activity of TGAs, we tested the DNA binding activity of TGAs to the target gene promoters by chromatin immunoprecipitation-polymerase chain reaction (ChIP-PCR) in the presence or absence of RipAB (Figure 6C). In WT plants, TGA2 bound to the cognate TGACG DNA-binding motif in the *SARD1* and *WRKY70* promoters upon INA treatment. The INA-induced TGA2 enrichment was comparable when co-expressing RipAB and the GFP control (Figure 6D). Similarly, the affinity of TGA2 for the promoters of *RBOHD* and *RBOHF* was comparable with or without RipAB expression post INA treatment (Figure 6D). These data indicated the DNA binding activity of TGAs is not affected by the interaction with RipAB. This assay showed similar results with TGA1 (Supplemental Figure S7A). A

previous study reported that NPR3 and NPR4 function as transcriptional co-repressors dependent on TGA2, TGA5, and TGA6 (Ding et al., 2018). Here, we found NPR3 suppressed the promoter activity of *PR1* and *WRKY70* by 50% compared to control, but the expression of RipAB did not significantly influence the inhibitory effect of NPR3 (Supplemental Figure S7B).

When the SA level increases, NPR1 binds SA and enters the nucleus to recruit TGA2, TGA5, and TGA6, thus promoting the activation of defense gene transcription (Zhang and Li, 2019). We therefore checked whether RipAB could inhibit the INA-induced interaction between NPR1 and TGA2 by Co-IP assay. However, the association of TGA2-HA and NPR1-FLAG upon INA treatment was not affected by co-expression of RipAB (Figure 6E). Consistent with the Co-IP results, BiFC demonstrated that the INA-induced TGA2-nYFP and NPR1-cYFP interaction could be detected with or without RipAB co-expression (Supplemental Figure S7C). Recently, ENHANCED DISEASE SUSCEPTIBILITY1 (*EDS1*) was shown to be a transcriptional coactivator to modulate gene expression by interacting with NPR1 (Chen et al., 2021). RipAB did not influence association of NPR1 and *EDS1*, as demonstrated by Co-IP assay in *Arabidopsis* protoplasts (Figure 6F). Taken together, these data indicated RipAB does not influence INA-induced NPR1 and TGA2 complex formation.

Gene expression requires transcriptional machinery and RNA Pol II to initiate and coordinate transcription. To investigate whether RipAB affects the ability of TGA-related transcription complex to recruit RNA Pol II, we monitored the association between TGA2 and RNA Pol II with or without RipAB. An enhancement of the association between TGA2 and RNA Pol II could be detected upon INA treatment, but this was abolished in the presence of RipAB (Figure 6G). Similarly, the INA-induced association of TGA6 and RNA Pol II was blocked by RipAB (Supplemental Figure S7D).

Furthermore, we checked the enrichment of RNA Pol II to the promoters of TGA2 target genes by ChIP-PCR in WT and RipAB overexpression plants. In WT plants, RNA Pol II bound to the TATA box around the transcription start site in the core promoter of *PR1* upon INA treatment; however, the INA-induced RNA Pol II enrichment was reduced by 50% in *oxRipAB* plants compared with WT (Figure 6G). Similarly, we also observed the reduced enrichment of RNA Pol II on the *RBOHD* and *RBOHF* promoters (Supplemental Figure S7E). To explore whether this phenomenon is related to TGAs, we tested RNA Pol II enrichment in the *tga2/5/6* mutant. The enrichment of RNA Pol II on the promoters of key target genes *PR1*, *RBOHD*, and *RBOHF* was reduced in *tga2/5/6* triple mutants (Supplemental Figure S7F). These results revealed that RipAB affects the ability of the TGA-related transcription complex to recruit RNA Pol II through interacting with TGA transcription factors.

## Discussion

The destructive phytopathogen *R. solanacearum* deploys type III secreted effectors to impair plant immunity and

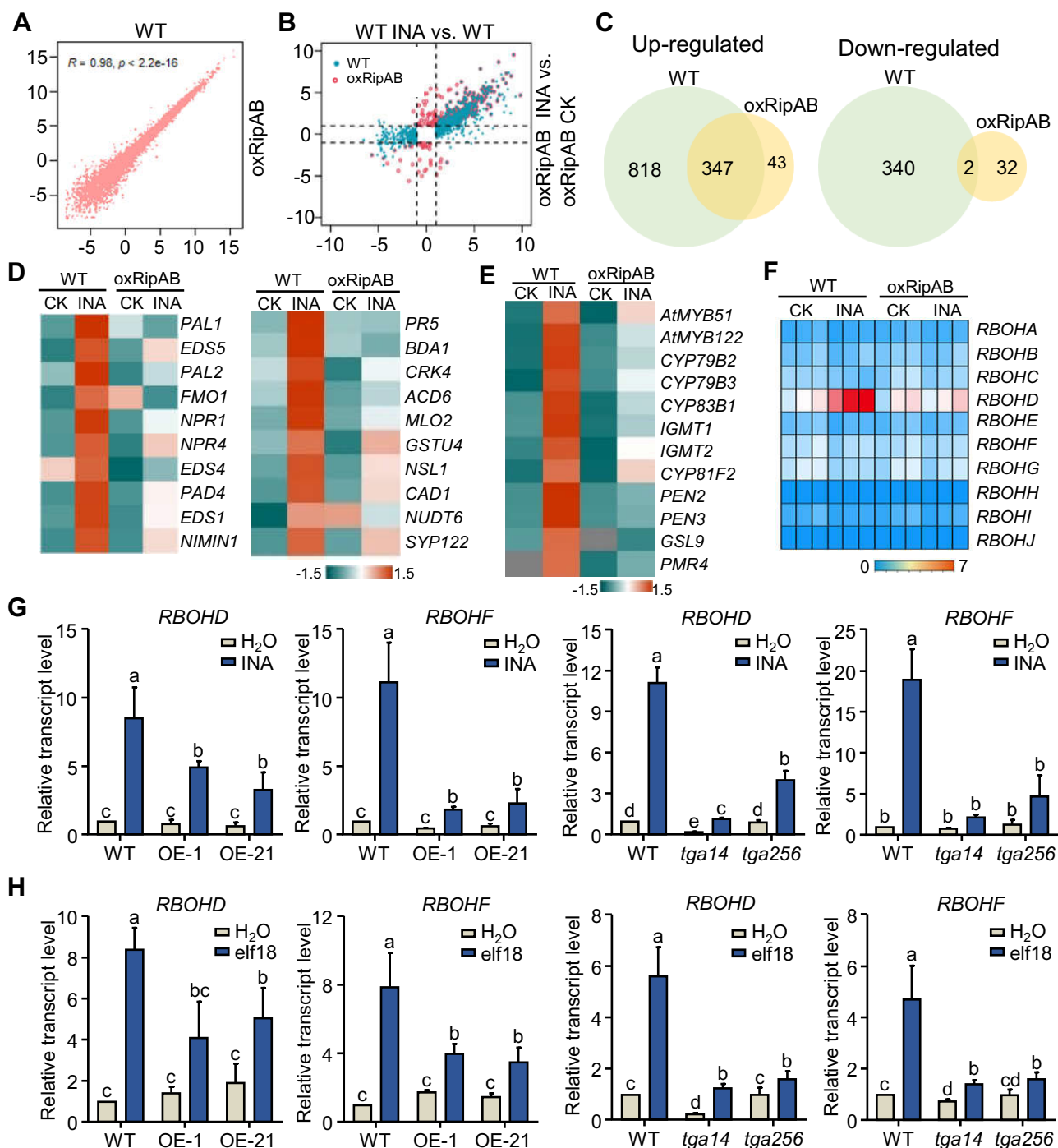


**Figure 5** RipAB affects INA-induced global gene transcription. **A**, Scatter plots of whole-genome transcripts fragments per kilobase of transcript per million mapped reads in WT versus RipAB overexpression plants. Gene expression levels were detected in 10-day-old seedlings without treatment. The x-axis indicates gene expression in WT and the y-axis indicates gene expression in RipAB overexpression plants. **B**, Scatter plots of DEGs in WT and RipAB overexpression plants at 1 h after 250- $\mu$ M INA treatment. The x-axis indicates DEGs in WT and the y-axis indicates DEGs in RipAB overexpression plants. **C**, The number of INA-regulated genes in RipAB overexpression plants is greatly reduced than that in the WT. The upregulated genes and downregulated genes were calculated in accordance with fold change  $\geq 2$  and FDR  $< 0.05$ . **D**, Heatmap cluster of INA-induced SA signaling and downstream target genes in WT and RipAB overexpression plants. The corresponding genes are listed on the right. **E**, Heatmap cluster of INA-induced callose biosynthesis-related genes in WT and RipAB overexpression plants. The corresponding genes are listed on the right. **F**, Gene expression pattern of the *RBOH* family members in WT and RipAB overexpression plants. **G**, INA-induced *RBOHD* and *RBOHF* expression are suppressed in RipAB overexpression lines and *tga* mutants. Seedlings were treated with 250- $\mu$ M INA or ddH<sub>2</sub>O for 6 h for RT-qPCR analysis. **H**, Elf18-induced *RBOHD* and *RBOHF* expression in RipAB overexpression lines and *tga* mutants by RT-qPCR analysis. Seedlings were treated with 100-nM elf18 or ddH<sub>2</sub>O for 6 h. The above experiments were repeated at three times with similar results. Error bars in (G) and (H) represent means  $\pm$  sd of three technical replicates from one biological repeat and different letters are used to indicate samples with significant differences (one-way ANOVA,  $P < 0.05$ ).

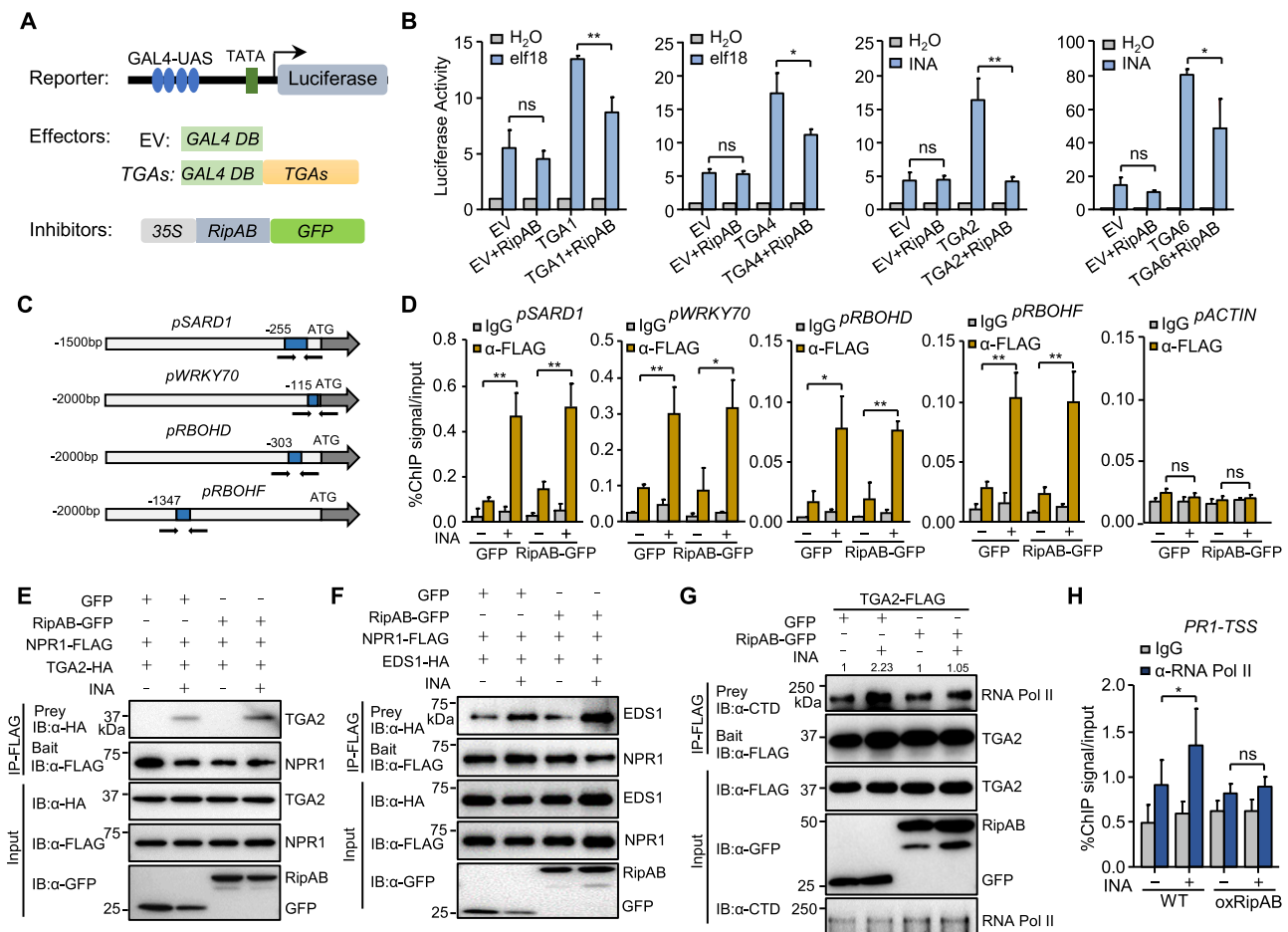


**Figure 6** RipAB suppresses TGAs transcriptional activity. **A**, Schematic diagram of the reporter, effector and inhibitor constructs used in the transcriptional activity assay. The reporter construct consists of four copies of GAL4-UAS, a minimal 35S promoter, and a LUC reporter gene. The effector constructs contain sequences encoding GAL4 DNA binding domain alone (Ctrl) or with TGAs under the control of 35S promoter. **B**, RipAB inhibits TGAs transcriptional activity. The reporter vector was co-transfected with depicted effector and inhibitor constructs in Arabidopsis protoplasts. Samples were treated with or without 100-nM eIF18 or 100- $\mu$ M INA. *UBQ-GUS* was included as an internal control. Error bars represent  $\pm$ SD of three biological replicates. **C**, Schematic diagram of *SARD1*, *WRKY70*, *RBOHD*, and *RBOHF* promoters with the positions of PCR primers for the ChIP assays. The orange boxes represent the cis-elements for TGA binding. **D**, RipAB does not influence the TGA2 binding activity by ChIP-PCR. Arabidopsis protoplasts co-expressing TGA2-FLAG with RipAB-GFP or GFP were treated with or without 100- $\mu$ M INA for 1 h. ChIP results were analyzed by quantitative PCR using specific genes. IgG and *ACTIN 12* were used as negative control. **E**, RipAB does not influence INA-induced interaction between NPR1 and TGA2. NPR1-FLAG and TGA2-HA were co-expressed with GFP only or RipAB-GFP in Arabidopsis protoplasts with or without 100- $\mu$ M INA for 15 min. Total protein extracts were immunoprecipitated with FLAG-trap beads and immunoblotted using an  $\alpha$ -HA or  $\alpha$ -FLAG antibody. Protein inputs are shown with immunoblotting before immunoprecipitation (bottom three parts). **F**, RipAB does not affect the interaction of NPR1 and EDS1. NPR1-FLAG and EDS1-HA were co-expressed with GFP only or RipAB-GFP in Arabidopsis protoplasts with or without 100- $\mu$ M INA. **G**, RipAB influences INA-induced interaction between RNA polymerase II and TGA2. TGA2-FLAG were co-expressed with GFP or RipAB-GFP in Arabidopsis protoplasts with or without 100- $\mu$ M INA. Total protein extracts after 0.5-h treatment were immunoprecipitated with  $\alpha$ -FLAG Agarose and immunoblotted using indicated antibodies. **H**, RipAB inhibits the ability of TGAs to recruit RNA polymerase II to *PR1* promoter. The seedlings of WT and RipAB overexpression line were treated with 250- $\mu$ M INA or ddH<sub>2</sub>O for 1 h. Chromatin complexes were immunoprecipitated using antibody against RNA polymerase II-CTD. qPCR was performed to detect the *PR* promoter bound by RNA polymerase II using specific primers. The above experiments were repeated at three times with similar results. Data in (D) and (H) represent the mean  $\pm$  SD of three technical replicates from one biological repeat. Asterisk indicates a significant difference (Student's *t* test, \**P* < 0.05, \*\**P* < 0.01) when compared with control.

achieve virulence, but the mechanism has not been fully uncovered. In this study, we demonstrated that the plant nuclear-localized T3E RipAB, one of the core type III effectors in *R. solanacearum*, targets multiple host TGA factors

to dampen immunity. RipAB is essential for *R. solanacearum* virulence and in planta expression of RipAB compromises plant resistance against *R. solanacearum* and *P. syringae*. Significantly, RipAB inhibits the expression of immune



responsive genes by impairing the transcriptional activity of TGAs, eventually leading to compromised resistance. In particular, the key phytohormone SA signaling pathway was disrupted by this bacterial effector (Figure 7). The *ripAB* homolog in *R. solanacearum* potato phylotype II strain UW551 was shown to be required for its virulence to potato (*Solanum tuberosum*; Zheng et al., 2019), suggesting that RipAB has key, evolutionarily conserved functions to manipulate host defenses and facilitate pathogen infection.

Some effectors enter the plant nucleus to affect host gene expression; this effective strategy can globally weaken the plant immune system. For example, the well-studied *Xanthomonas* TALE effectors carry a DNA binding domain and NLS sequence, and target and activate the expression of host susceptibility genes (Perez-Quintero and Szurek, 2019). Recently, one TALE-LIKE effector in *R. solanacearum* was reported to subvert translational regulation to boost host polyamine levels, thereby triggering a defense reaction and likely inhibiting bacterial niche competitors (Wu et al., 2019). Another *R. solanacearum* acetyltransferase effector, PopP2, acetylates multiple defense-related WRKY transcription factors in the plant nucleus, causing a loss of WRKY-DNA binding and transactivating functions needed for defense gene expression and disease resistance (Sarris et al., 2015). Here, we found that RipAB enters the plant nucleus to suppress immune gene expression by interacting

and interfering with TGA transcriptional factors. In particular, *R. solanacearum* was unable to suppress TGA-regulated immune gene induction in the absence of RipAB during root infection (Supplemental Figure S8). Thus, we revealed a strategy by which *R. solanacearum* dampens plant immunity through a plant-nuclear localized effector.

There are 10 TGAs in Arabidopsis, and these were classified into five clades, among which the function of clades I and II TGAs in different plant defense pathways has been well characterized (Gatz, 2013; Zhang and Li, 2019). The clade II members TGA2, TGA5, and TGA6, originally identified in a screen for NPR1-interacting proteins, are crucial in establishing SAR response (Zhang et al., 1999; Zhou et al., 2000). In contrast, the clade I members TGA1 and TGA4 and the clade III member TGA3 are involved in basal resistance against pathogens (Zhang et al., 2003; Shearer et al., 2012; Sun et al., 2018). In addition, TGA1 and TGA4 regulate the biosynthesis of pipecolic acid and SA, which is crucial for SAR (Sun et al., 2018). We found that RipAB targets TGA1–TGA7, indicating RipAB could interfere with diverse branches of plant immunity. Notably, transgenic plants with RipAB expression resemble the immune defect phenotypes of *tga* mutants including PTI, basal defense, and SAR. The *tga1 tga4* double mutants are more susceptible to *R. solanacearum* infection. In addition, consistent with our biochemical data on direct RipAB–TGA interactions, the

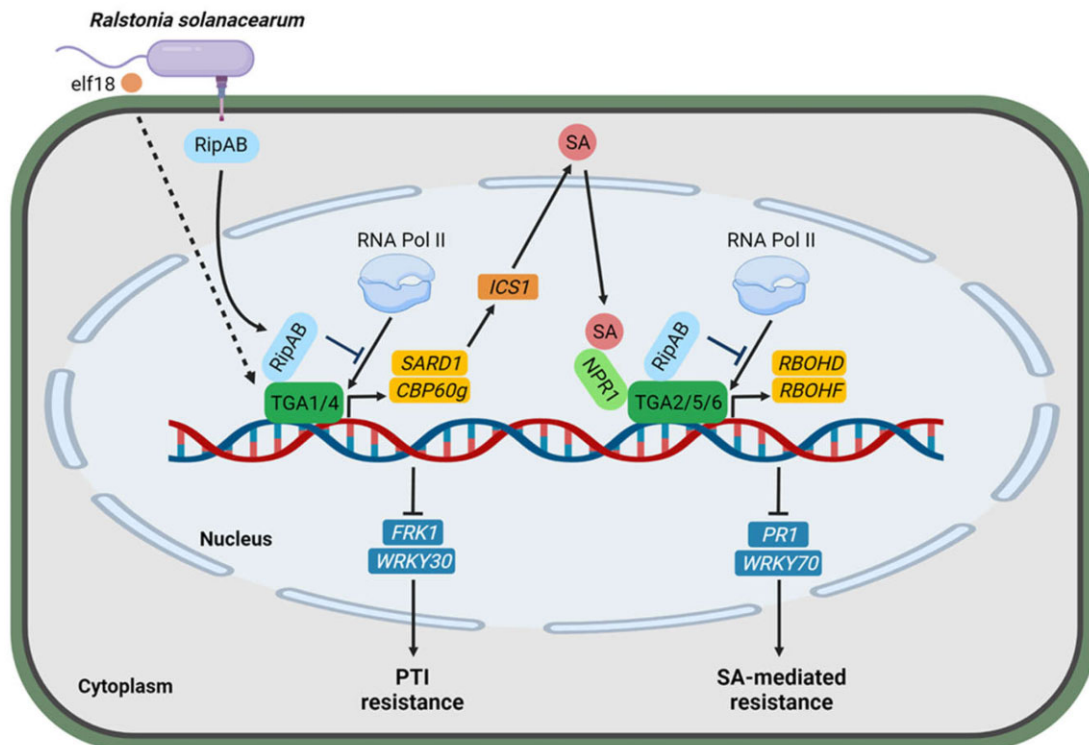


**Figure 7** A working model of *R. solanacearum* effector RipAB subverting plant immunity. The *R. solanacearum* core effector RipAB is secreted into the plant cell by type III secretion system and translocated in the plant nucleus. RipAB interacts with transcription factors TGA1 and TGA4, leading to the suppression of the PAMP-triggered resistance, as well as pipecolic acid and SA biosynthesis gene expression. RipAB also interacts with TGA2, TGA5, and TGA6, causing the compromised SA-triggered responses. RipAB inhibits TGA function through interfering with the ability of transcriptional complex to recruit RNA polymerase II.

compromised virulence of the *Δripab* strain on Arabidopsis was significantly recovered in the absence of TAG2/TGA5/TGA6 and slightly restored in the *tga1 tga4* double mutant. Therefore, these physical and biological data suggest that TGAs are the major virulence targets of RipAB. Our study thus reveals that a pathogen effector targets this key group of transcription factors in plant immunity. Since RipAB is conserved in all *R. solanacearum* phylotypes and RipAB activity is indispensable for plant infection, these findings may help researchers develop effective strategies to combat this devastating pathogen, such as modifying TGAs to escape from being targeted by RipAB, and developing RipAB inhibitors.

Disrupting the homeostasis of plant defense-related hormone signaling is a conserved mechanism for pathogens to suppress defense. Since SA signaling is crucial for plant resistance to diverse pathogens, these pathogens deploy various factors to inhibit SA biosynthesis and signaling (Qi et al., 2018). Coronatine, a bacterial phytotoxin that is structurally related to JA, mimics JA function to activate the JA pathway, thus disrupting SA signaling (Zheng et al., 2012). HopX1, a *P. syringae* effector with cysteine protease activity, promotes the degradation of JAZ proteins, thus leading to the activation of JA signaling, which in turn suppresses SA signaling (Gimenez-Ibanez et al., 2014). The SA receptor NPR1 could be ubiquitinated by the *P. syringae* effector AvrPtoB. The subsequent degradation of NPR1 blocks SA perception to reduce plant resistance (Chen et al., 2017). As the core transcription factors, TGA2, TGA5, and TGA6 have been shown to physically interact with NPR1 and NPR3/4 *in planta*, and are critical for SA-related defense gene expression (Zhang et al., 2003). Based on our RNA-seq analysis, a large portion of SA-upregulated genes are less induced or uninduced in RipAB-overexpressing plants. Together with the observation that RipAB overexpression lines are more sensitive to toxicity of SA and lost SA-induced resistance to DC3000, these data indicated that the SA pathway is suppressed in the presence of RipAB. Interestingly, beside their originally identified roles in SAR or basal defense, we found that TGAs are required for certain branches of early immune responses. These may be because of the positive feedback regulation of SA on PRR-related immunity. For instance, SA could enhance PAMP-induced responses including ROS burst and callose deposition, which may be due to the increased levels of PRRs (Tateda et al., 2014). Here, we found that INA treatment induces upregulation of *RBOHD* and *RBOHF* that depend on TGAs. Furthermore, we identified the promoters of *RBOHD* and *RBOHF* as direct binding targets of TGAs. INA and elf18-induced *RBOHD/F* expression was suppressed in the presence of RipAB, which acted by interfering with TGA function. Our study revealed a mechanism by which a bacterial pathogen suppresses SA-mediated resistance and ROS production. It is noted that the basal expression level of *RBOHD* was comparable in WT and oxRipAB plants (Supplemental Data Set 2), which could not fully explain how RipAB suppresses the PAMP-triggered ROS burst, an

early PTI event and peaking within 15 min. However, since RipAB targets TGAs to influence a range of gene expression, it is likely that other genes involved in ROS burst regulation are suppressed by RipAB or in TGA mutants.

Although RipAB targets TGA transcription factors and suppresses downstream immune gene expression, the hijacking molecular mechanism remains to be characterized. Gene transcription is a complex event that needs to recruit general and specific transcription units as well as RNA Pol II (Li et al., 2016). As a transcriptional activator, NPR1 interacts with clade II TGA transcription factors via the ankyrin repeats upon SA perception (Zhang et al., 1999; Zhou et al., 2000). Meanwhile, NPR1 and the CBP/p300-family HACs form a coactivator complex. The HAC–NPR1–TGA complex activates *PR* gene transcription by histone acetylation-mediated epigenetic reprogramming (Jin et al., 2018). First, our data showed that the transcriptional activity of TGAs is greatly inhibited in the presence of RipAB. However, RipAB does not interfere with the affinity of TGA1 and TGA2 for the TGACG element in the promoters of their target genes, such as *WRKY70* and *SARD1* (Ding et al., 2018; Sun et al., 2018). In addition, we found SA-induced NPR1–TGA2 and NPR1–EDS1 protein complexes are not influenced by RipAB. The inhibition of TGA transcription activity by RipAB could result from the suppression of either RNA Pol II recruitment or transcription initiation. We finally found that RipAB inhibits the occupation of RNA Pol II around the transcription start site of TGA regulons, likely through targeting TGA transcription factors. The data could also rule out the possibility that RipAB prohibits the release of Pol II from the promoters for transcription initiation. Whether RipAB influences the step of recruiting other transcription machinery components into NPR1–TGA complex, such as mediators and histone modification enzymes, will be further explored. It is worthwhile to reveal the detailed differences of NPR1–TGA1 transcription machinery with and without RipAB. The related results also will help us to understand the mechanisms of TGA-mediated transcriptional reprogramming and identify important components downstream of SA signaling pathway.

## Materials and methods

### Plant materials and growth conditions

All *A. thaliana* plants used in this study were in the Columbia-0 (Col-0) background. *tga1 tga4* and *tga2 tga5 tga6* mutants were kindly provided by Dr Yuelin Zhang. Arabidopsis lines were grown in soil in a growth room at 22°C, 75  $\mu\text{E}\cdot\text{m}^{-2}\cdot\text{s}^{-1}$  (T5 LED Tube Lights, 4000K) with 12-h light/12-h dark photoperiod, and 45% relative humidity. Arabidopsis seedlings were germinated on half-strength Murashige and Skoog (MS) plates containing 1% (w/v) sucrose and 0.8% (w/v) agar and grown for 10 days. *Nicotiana benthamiana* plants were grown in jiffy pots in a growth room at the same condition described above. Four-week-old *N. benthamiana* leaves were used for *Agrobacterium*-mediated transformation assays. *Solanum lycopersicum* cv. Money

Maker were sown and cultivated under the same conditions.

### Bacterial strains

*Ralstonia solanacearum* strains GMI1000, *RipAB* mutants  $\Delta ripab-1$  and  $\Delta ripab-2$  were grown on CPG solid medium and cultured at 28°C in CPG liquid medium. *Pseudomonas syringae* pv. *tomato* (*Pst*) strains *Pst* DC3000 and *Pst* DC3000 *hrcC* were cultured at 28°C in King's B (KB) medium containing 50  $\mu\text{g}\cdot\text{mL}^{-1}$  rifampicin, *Pst* DC3000 carrying *avrRpt2* were cultured overnight at 28°C in KB medium with 50  $\mu\text{g}\cdot\text{mL}^{-1}$  rifampicin and kanamycin. *Pseudomonas syringae* pv. *maculicola* *Psm* ES4326 were cultured overnight at 28°C in KB medium containing 50  $\mu\text{g}\cdot\text{mL}^{-1}$  rifampicin and streptomycin. *Agrobacterium tumefaciens* strain GV3101 carrying different constructs were cultured in LB medium with 25  $\mu\text{g}\cdot\text{mL}^{-1}$  gentamicin and respective antibiotics at 28°C.

### Plasmid construction

The *RipAB* coding sequence was amplified from *R. solanacearum* strain GMI1000 genomic DNA with primers containing Xba I at N terminus and Stu I at the C terminus and introduced into the *pC007* blunt vector (Tsingke, TSV-007), then the *RipAB* gene was subcloned into *pHBT* vectors driven by CaMV 35S promoter with an HA, FLAG, or GFP tag at C terminus for protoplasts transient expression assay. *RipAB* gene was subcloned into binary expression vectors driven by CaMV 35S promoter for assays in *N. benthamiana* and *Agrobacterium*-mediated floral dipping of Arabidopsis, *RipAB* gene was also subcloned into *pMBP* vector for expression in *Escherichia coli*. *RipAB* nuclear localization mutants *RipAB*<sup>4KA</sup>, *RipAB*<sup>5KA</sup>, and *RipAB*<sup>ns</sup> were generated by site-directed mutagenesis method, and the corresponding vectors for protoplasts transient expression and assays used in *N. benthamiana* were constructed using the same methods. The other candidate effectors were also amplified from *R. solanacearum* strain GMI1000 genomic DNA with primers as listed in Supplemental Table S1 and subcloned into *pHBT* vector with an HA tag. The genes encoding *AtTGAs* were amplified from Arabidopsis Col-0 cDNA and subcloned into *pHBT* or binary expression vectors driven by CaMV 35S promoter. *AtNPRs* and *AtEDS1* were amplified from Arabidopsis Col-0 cDNA and were subcloned into *pHBT* vector driven by CaMV 35S promoter for assays in protoplasts via homologous recombination method (Vazyme, Cat. C113-02).

### Generation of transgenic plants and *R. solanacearum* knockout mutants

*Agrobacterium tumefaciens* GV3101 carrying the binary constructs *pTF101-RipAB-GFP* or *pTF101-RipAB*<sup>ns</sup>-*GFP* under 35S promoter were cultured overnight at 28°C in LB liquid medium with 25  $\mu\text{g}\cdot\text{mL}^{-1}$  gentamicin and 25  $\mu\text{g}\cdot\text{mL}^{-1}$  spectinomycin. After centrifuging for 5 min at 4,000 rpm, bacteria were suspended with *Agrobacterium* infiltration buffer containing 50-mM MES (pH 5.5–5.7), 5% sucrose, and 200  $\text{mL}\cdot\text{L}^{-1}$  silwetL-77 at the density of optical density (OD)<sub>600</sub> = 0.8. Arabidopsis flower buds were dipped

thoroughly to the bacteria suspension and the dipped plants were moisturized for 12 h, then the plants were grown in a 12-h light/12-h dark photoperiod, 75  $\mu\text{E}\cdot\text{m}^{-2}\cdot\text{s}^{-1}$ , 22°C, and 45% relative humidity condition for seeds harvesting. Transgenic Arabidopsis plants were selected with basta spraying and were further confirmed by immunoblot using  $\alpha$ -GFP antibody (Roche, Cat.11814460001).

To generate *R. solanacearum*  $\Delta ripab$  mutants, the *RipAB* coding sequence was replaced by kanamycin resistance cassette with homologous recombination method. The *RipAB* flanking regions, upstream (UP) and downstream (DN) with part of kanamycin fragment, were amplified by PCR and merged with kanamycin resistance gene by PCR. The resulting fusion UP-KAN-DN fragment was introduced into *R. solanacearum* GMI1000 strain by electroporation transformation. The  $\Delta ripab$  mutants were selected using kanamycin (25  $\mu\text{g}\cdot\text{mL}^{-1}$ ) and confirmed by PCR using specific primers for the *RipAB* gene and *R. solanacearum* flagellum protein. To complement *RipAB* in the  $\Delta ripab$  mutant, the *RipAB* promoter from *RipABC* operon was cloned into *pHM1*, after which the *RipAB* coding region with HA tag were introduced to create an intact *pHM1-pRipAB-RipAB-HA* construct. Then the construct was introduced into  $\Delta ripab$  mutant by electroporation transformation. The complementation strain was selected using kanamycin and spectinomycin (25  $\mu\text{g}\cdot\text{mL}^{-1}$ ) and confirmed by PCR using specific primers for the *RipAB* gene and western blotting with  $\alpha$ -HA antibody (Roche, Cat. 12013819001).

### Bacterial inoculation assays

Soil drenching inoculation was performed for *R. solanacearum* inoculation assay, 20-mL *R. solanacearum* suspension with OD<sub>600</sub> = 0.1 was poured onto the wounded roots of Arabidopsis and tomato plants at 4-week-old. The plants were kept in a growth incubator at 75% humidity, 12-h light/12-h dark photoperiod, and 28°C for disease symptom scoring according to a scale ranging from 0 to 4 (0: no wilting; 1: 1%–25% wilting; 2: 26%–50% wilting; 3: 51%–75% wilting; 4: 76%–100% wilting). Bacterial populations were detected at 3–6 dpi, Arabidopsis plant roots from six independent plants were weighed for bacteria quantification, then the root tissues were ground in 100- $\mu\text{L}$  ddH<sub>2</sub>O and 10  $\mu\text{L}$  of diluted solution was spread on solid CPG medium. For bacteria quantification in tomato stems, 1-cm-long tissues above stem base were ground in ddH<sub>2</sub>O and diluted solution was spread on solid CPG medium with appropriate antibiotics, CFUs were counted after 2 days culture at 28°C.

For *P. syringae* inoculation, *Pst* and *Psm* strains were cultured overnight at 28°C in KB medium with appropriate antibiotics. Bacteria were resuspended in 10-mM MgCl<sub>2</sub> at desired density. Four-week-old plants leaves were infiltrated with the bacterial suspension and collected to measure bacterial populations, eight leaf discs separated as four repeats were ground in 100- $\mu\text{L}$  ddH<sub>2</sub>O, and serial dilutions were plated onto TSA medium with the appropriate antibiotics. CFUs were counted after 2 days culture at 28°C.



### ROS assay and MAPK assay

Leaves from 4-week-old *Arabidopsis* plants for each genotype were excised into leaf discs of 0.25 cm<sup>2</sup> and cut into leaf strips, followed by incubation overnight in 96-well plates with 100- $\mu$ L ddH<sub>2</sub>O to eliminate the wounding effect. Before detection, 100- $\mu$ L reaction solution containing 50- $\mu$ M luminol (Sigma, Cat. A8511) and 10- $\mu$ g·mL<sup>-1</sup> horseradish peroxidase (Sigma, Cat. P6782) with appropriate elicitors were added to 96-well plates. The measurement was carried out immediately after adding the solution with a Multimode Reader Platform (Tecan Austria GmbH, SPARK 10M) for a period of 30 min, the values of ROS production represent the relative light units of different plants. For ROS assay in *N. benthamiana*, *Agrobacterium*-mediated transient expression was performed first, then ROS production was detected using the same method as above.

Ten-day-old seedlings were transferred to the 12-well plate with 500- $\mu$ L ddH<sub>2</sub>O for overnight-recovery and then treated with 100-nM elf18 for 0, 5, 15, and 30 min. Samples were ground in protein extraction buffer (20-mM Tris-HCl, pH 7.5, 100-mM NaCl, 1-mM EDTA, 10% glycerol, and 1% Triton X-100) and boiled at 95°C for 10 min. Supernatant was collected after 12,000 rpm centrifugation for 5 min and protein samples with sodium dodecyl sulphate (SDS) buffer were loaded on 10%SDS-polyacrylamide gel electrophoresis (SDS-PAGE) gel to detect pMPK3, pMPK4, and pMPK6 by immunoblot with  $\alpha$ -pERK1/2 antibody (CST, Cat. 9101S).

### Callose deposition assay

Leaves from 5-week-old plants grown in soil were infiltrated with ddH<sub>2</sub>O or 500-nM elf18. After treatment for 24 h, leaves were transferred into the fixing solution containing 10% formaldehyde, 5% acetic acid, and 50% ethanol for 12 h and destained in 95% ethanol for 6 h. The clear leaves were washed twice with 70% ethanol and three times with ddH<sub>2</sub>O water, and then dipped in 0.01% aniline blue solution (150-mM KH<sub>2</sub>PO<sub>4</sub>, pH 9.5) for 15 min for callose staining. Callose deposition was detected with a fluorescence microscope (Leica, DM2500).

### Reporter assay and transcriptional activity assay

LUC reporter assay was performed using *Arabidopsis* protoplasts by transforming the effector constructs driven by 35S promoter and firefly LUC reporter constructs driven by indicated immune maker gene promoter. After 4 h incubation, samples were treated with 100-nM elf18 or 100- $\mu$ M INA (2,6-dichloroisonicotinic acid, Sigma, Cat. 456543) for another 4 h. *UBQ10-GUS* was included in the assay as an internal transfection control. After incubation, protoplasts were collected and suspended with cell lysis buffer (25-mM Tris-phosphate, pH 7.8, 2-mM 1,2-diaminocyclohexane-N,N,N',N'-tetraacetic acid, 10% glycerol, 1% Triton X-100, and 2 mM DTT). The Multimode Reader Platform (Tecan, SPARK 10M) was used to measure the LUC activity with the LUC assay substrate (Promega, Cat. E1501). For the GUS activity, methylumbelliferyl- $\beta$ -D-glucuronide was mixed with the lysed cells, and the fluorescence signals were analyzed

with a Multilabel plate Reader (Tecan, SPARK 10M). The ratio of LUC/GUS activity was used to calculate the relative LUC activities.

Transcriptional activity assay was performed using *Arabidopsis* protoplasts by transforming the reporter, effector, and inhibitor constructs. *UBQ10-GUS* was included in the assay as an internal transfection control. After transformation, the protoplasts were treated with or without 100- $\mu$ M INA immediately for 12 h, then protoplasts were collected and resuspended with cell lysis buffer. LUC and GUS activities were measured to calculate the relative LUC activities.

### RNA isolation and RT-qPCR analysis

Total RNA was isolated from 10-day-old *Arabidopsis* seedlings grown on half-strength MS medium or leaf discs of 4-week-old *Arabidopsis* plants grown in soil with Trizol reagent from TIANGEN (Cat. DP424). Total RNA was reverse transcribed to synthesize first-strand cDNA at 50°C for 30 min after treatment with RNase-free DNase I at 42°C for 2 min (Vazyme, Cat. R223-01). Reverse transcription quantitative RT-qPCR analysis was carried out using SYBR green Supermix (Monad, Cat. MQ00401S) with the gene specific primers (Supplemental Table S1) on the BIO-RAD CFX96 Touch System following standard protocol. The expression of each gene was normalized to the expression of *ACTIN2*.

### RNA sequencing and data analysis

Ten-day-old *Arabidopsis* seedlings grown on half-strength MS medium were used for RNA-seq analysis. Library construction and Illumina sequencing were performed by Berry Genomics (Wuhan, China). Sequencing reads were mapped to the Col-0 genome (TAIR10) using Hisat2 (Kim et al., 2015). Uniquely mapped reads with up to two mismatches were retained. Read counts of each gene were calculated using FeatureCounts (Liao et al., 2014). Gene expression levels were normalized into fragments per kilobase of transcript per million using R package limma (Ritchie et al., 2015). DEGs were identified using DESeq2 (Love et al., 2014) with default settings. Genes with two-fold or more changes in gene expression levels and *q*-value < 0.05 (FDR, corrected from *P*-values by the Benjamini-Hochberg testing) were considered as DEGs.

### Co-IP assay

*Arabidopsis* protoplasts were transfected with indicated plasmids and incubated for 12 h before treated with or without 100- $\mu$ M INA, then samples were collected by centrifugation and lysed with Co-IP buffer containing 20-mM Tris-HCl, pH 7.5, 100-mM NaCl, 1-mM EDTA, 2-mM DTT, 10% glycerol, 0.5% Triton X-100, and protease inhibitor cocktail (Roche, Cat. 04693116001) by vortexing. Before co-IP, total protein extracts were pre-incubated with protein G agarose beads (Millipore, Cat. 16-201) at 4°C for 1 h, then immunoprecipitation was performed with  $\alpha$ -FLAG agarose (Sigma, Cat. A2220) or  $\alpha$ -GFP agarose (Chromo Tek, Cat. gta-20) at 4°C for 3 h. The agarose beads were collected and washed

three times with washing buffer containing 20-mM Tris-HCl, pH 7.5, 100-mM NaCl, 1-mM EDTA, and 0.1% Triton X-100. The immunoprecipitated proteins and input proteins were analyzed by immunoblotting with indicated antibodies.

### Agrobacterium-mediated transient expression in *N. benthamiana*

Binary vectors were introduced into *A. tumefaciens* strain GV3101 by electroporation. Before infiltration, the *Agrobacterium* cell suspension was treated with 200- $\mu$ M acetosyringone (Sigma, Cat. D134406) for 3 h. Bacterial suspension was adjusted to a final density at  $OD_{600} = 1.5$ . Samples were taken 1–3 dpi for analysis based on experimental requirements.

### Large-scale immunoprecipitation and LC-MS/MS analysis

*Nicotiana benthamiana* leaf tissues were collected 2 days after infiltration with *Agrobacterium* carrying *RipAB-GFP* constructs and frozen in liquid nitrogen. The tissues were lysed with Co-IP buffer containing 20-mM Tris-HCl, pH 7.5, 100-mM NaCl, 1-mM EDTA, 2-mM DTT, 10% glycerol, 0.5% Triton X-100, and protease inhibitor. After centrifuging for 15 min, supernatant was incubated with 20- $\mu$ L GFP-Trap beads (Chromo Tek, Cat. gta-20) at 4°C for 3 h. Then the agarose beads were collected and washed three times with Co-IP washing buffer containing 20-mM Tris-HCl, pH 7.5, 100-mM NaCl, 1-mM EDTA, 0.1% Triton X-100, and protease inhibitor. The protein extracts separated by SDS-PAGE were collected for identification of interacting proteins, Mass Spectrometric analysis were performed by APPLIED PROTEIN TECHNOLOGY (Shanghai, China).

### Confocal microscopy and image analysis

For subcellular localization assay in protoplasts, desired constructs fusions were transfected into protoplasts from 4-week-old Arabidopsis plants. After incubation for 12 h, fluorescence signals were observed with confocal microscopy. For BiFC assay, *A. tumefaciens* strain GV3101 carrying the desired constructs were hand-infiltrated into *N. benthamiana* leaves, YFP fluorescence signals in the *N. benthamiana* leaf discs were examined at 1–2 dpi with confocal microscopy (Leica, SP8). For split-LUC assay, *A. tumefaciens* strain GV3101 containing the desired constructs were hand-infiltrated into *N. benthamiana* leaves. Split-luciferase assays were carried out both qualitatively and quantitatively at 1–2 dpi, respectively. For the CCD imaging, the *N. benthamiana* leaves were smeared with 1-mM luciferin (YEASEN, Cat. 40902ES01) dilution and kept in the dark for 5 min before charge coupled device (CCD) imaging. The images were taken with Chemiluminescence Apparatus (Tanon, 5200 Multi). To quantify the LUC signal, 0.25-cm<sup>2</sup> leaf discs sprayed with 1-mM luciferin dilution were collected into a 96-well plate to record the luminescence with a Multimode Reader Platform (Tecan, SPARK 10M).

### In vitro pull-down assay

GST or GST-TGAs, GST-TGA2C, GST-TGA2N, and MBP-RipAB-HA fusion proteins were expressed in the *E. coli* strain BL21 and purified through affinity chromatography with glutathione agarose (Thermo, Cat. 16102BID) or amylose resin (NEB, Cat. E8021S) according to standard protocols. MBP fusion protein MBP-RipAB-HA were pre-incubated with pre-washed glutathione agarose in 300- $\mu$ L incubation buffer (20-mM Tris-HCl, pH 7.5, 100-mM NaCl, 0.1-mM EDTA, and 0.5% Triton X-100) at 4°C for 30 min, then the supernatant was collected by centrifugation and incubated with pre-washed GST, GST-TGAs, GST-TGA2N, or GST-TGA2C beads at 4°C for another 1–2 h. The beads were collected and washed three times with washing buffer (20-mM Tris-HCl, pH 7.5, 300-mM NaCl, 0.1-mM EDTA, and 0.1% Triton X-100). Proteins were detected with  $\alpha$ -HA antibody by immunoblotting.

### ChIP assay

Arabidopsis protoplasts were transfected with indicated plasmids and incubated for 12 h, then protoplasts were treated with or without 100- $\mu$ M INA for 1 h before harvesting. WT and indicated transgenic seedlings were harvested following 1 h treatment by ddH<sub>2</sub>O or INA. For ChIP experiments, protoplasts or seedlings were cross-linked in 1% formaldehyde solution for 10 min, then 2-M glycine was added to a final concentration of 100 mM for 5 min to stop the cross-linking, and protoplasts were harvested without supernatant by centrifugation. The protoplasts were resuspended in nuclei isolation buffer (0.25-M sucrose, 10-mM Tris-HCl pH = 8, 10-mM MgCl<sub>2</sub>, 50-mM KCl, 1% Triton X-100, 1-mM PMSF, and protease inhibitors) and sonicated to shear the DNA to an average size of 0.2–0.5 kb. Immunoprecipitation was performed with IgG (ABclonal, Cat. AC005),  $\alpha$ -RNAPII CTD (Abcam, Cat. Ab26721) and followed with Protein G-Agarose (Millipore, Cat. 3241198) or  $\alpha$ -FLAG agarose (Sigma, Cat. A2220). Then the samples were reverse cross-linked and immunoprecipitated DNA was precipitated with ethanol following proteinase K digestion. At last, RT-qPCR analysis was carried out with specific primers (Supplemental Table S1) for amplifying the indicated gene promoter.

### Phylogenetic analysis

Sequence alignments of AtTGAs were performed with MAFFT and results have been provided as a supplemental file in FASTA format (Supplemental File S1). Phylogenetic analyses were conducted in MEGA4. The group A gene *AtAB15* of bZIP transcription factor superfamily was selected as outgroup. The evolutionary history was inferred using the Neighbor-Joining method. The optimal tree with the sum of branch length = 3.5223 is shown. The percentage of replicate trees in which the associated taxa clustered together in the bootstrap test (1,000 replicates) are shown next to the branches. The evolutionary distances were computed using the Poisson's correction method and are in the units of the number of amino acid substitutions per site. All positions

containing gaps and missing data were eliminated from the data set (complete deletion option). There were total of 299 positions in the final data set.

### Accession numbers

Sequence data in this article can be found in the *R. solanacearum* Database or Arabidopsis Information Resource under the following accession numbers: *RipAA* (RSc0608), *RipAB* (RSp0876), *RipAI* (RSp0838), *RipAX1* (RSc3290), *RipAX2* (RSp0572), *RipBA* (RSc0227), *RipP1* (RSc0826), *RipU* (RSp1212), *TGA1* (AT5G65210), *TGA2* (AT5G06950), *TGA3* (AT1G22070), *TGA4* (AT5G10030), *TGA5* (AT5G06960), *TGA6* (AT3G12250), *TGA7* (AT1G77920), *ASR3* (AT2G33550), *NPR1* (AT1G64280), *NPR3* (AT5G45110), *EDS1* (AT3G48090), *ACTIN2* (AT3G18780), *FRK1* (AT2G19190), *NHL10* (AT2G35980), *WRKY30* (AT5G24110), *PR1* (AT2G14610), *WRKY70* (AT3G56400), *RBOHD* (AT5G47910), *RBOHF* (AT1G64060), *SARD1* (AT1G73805), and *CBP60g* (AT5G26920). The RNA-seq data were deposited in the Gene Expression Omnibus (GSE179700) at the National Center for Biotechnology Information.

### Supplemental data

The following materials are available in the online version of this article.

**Supplemental Figure S1.** Candidate Type III effectors screened in this study.

**Supplemental Figure S2.** RipAB localizes in plant nucleus and suppresses immune gene expression.

**Supplemental Figure S3.** RipAB plays an important role in the virulence of *R. solanacearum*.

**Supplemental Figure S4.** TGA transcription factor family members interact with RipAB.

**Supplemental Figure S5.** Overexpression of RipAB compromises TGA1/TGA4-regulated plant immunity.

**Supplemental Figure S6.** Compromised PAMP- and SA-induced immunity in *tga* mutants.

**Supplemental Figure S7.** RipAB inhibits the recruitment of RNA polymerase II to TGA transcriptional complex.

**Supplemental Figure S8.** *R. solanacearum* suppresses immune gene expression during infection through RipAB.

**Supplemental Table S1.** Primers used in this study.

**Supplemental Data Set S1.** List of potential RipAB interacting partners identified by IP-MS/MS analysis.

**Supplemental Data Set S2.** Global gene expression level from RNA-seq.

**Supplemental Data Set S3.** INA upregulated DEGs in WT and oxRipAB transgenic plant.

**Supplemental Data Set S4.** INA downregulated DEGs in WT and oxRipAB transgenic plant.

**Supplemental File S1.** Sequence alignment corresponding to the phylogenetic tree in Supplemental Figure S4.

### Acknowledgments

We thank Dr Yuelin Zhang from University of British Columbia for the seeds of *tga1/tga4* and *tga2/tga5/tga6*

mutants, Drs Huilan Chen, Yangrong Cao, Taotao Wang from Huazhong Agricultural University for sharing the GMI1000 strain, split-LUC vectors, and tomato seeds, respectively. We thank Dr Kenichi Tsuda for critical reading of the manuscript and constructive suggestions.

### Funding

This work was supported by the National Natural Science Foundation of China (Grant no. 31970125), Fundamental Research Funds for the Central Universities, Huazhong Agricultural University Scientific & Technological Self-innovation Foundation (Grant no. 2017RC001), Pests and Diseases Green Prevention and Control Major Special Project (Grant no. 110202101045, LS-05).

*Conflict of interest statement.* None declared.

### References

- Angot A, Peeters N, Lechner E, Vaillau F, Baud C, Gentzittel L, Sartorel E, Genschik P, Boucher C, Genin S (2006) *Ralstonia solanacearum* requires F-box-like domain-containing type III effectors to promote disease on several host plants. *Proc Natl Acad Sci USA* **103**: 14620–14625
- Cao H, Bowling SA, Gordon AS, Dong X (1994) Characterization of an Arabidopsis mutant that is nonresponsive to inducers of systemic acquired resistance. *Plant Cell* **6**: 1583–1592
- Cao H, Glazebrook J, Clarke JD, Volko S, Dong XN (1997) The Arabidopsis NPR1 gene that controls systemic acquired resistance encodes a novel protein containing ankyrin repeats. *Cell* **88**: 57–63
- Chen H, Li M, Qi G, Zhao M, Liu L, Zhang J, Chen G, Wang D, Liu F, Fu ZQ (2021) Two interacting transcriptional coactivators cooperatively control plant immune responses. *Sci Adv* **7**: eabl7173
- Chen H, Chen J, Li M, Chang M, Xu K, Shang Z, Zhao Y, Palmer I, Zhang Y, McGill J, et al. (2017). A bacterial type III effector targets the master regulator of salicylic acid signaling, NPR1, to subvert plant immunity. *Cell Host Microbe* **22**: 777–788.e7.
- Deslandes L, Genin S (2014) Opening the *Ralstonia solanacearum* type III effector tool box: insights into host cell subversion mechanisms. *Curr Opin Plant Biol* **20**: 110–117
- Ding Y, Sun T, Ao K, Peng Y, Zhang Y, Li X, Zhang Y (2018) Opposite roles of salicylic acid receptors NPR1 and NPR3/NPR4 in transcriptional regulation of plant immunity. *Cell* **173**: 1454–1467.e15
- Dong XY, Hong ZL, Chatterjee J, Kim SH, Verma DPS (2008) Expression of callose synthase genes and its connection with Npr1 signaling pathway during pathogen infection. *Planta* **229**: 87–98
- Droge-Laser W, Snoek BL, Snel B, Weiste C (2018) The Arabidopsis bZIP transcription factor family—an update. *Curr Opin Plant Biol* **45**: 36–49
- Gatz C (2013) From pioneers to team players: TGA transcription factors provide a molecular link between different stress pathways. *Mol Plant Microbe Interact* **26**: 151–159
- Genin S, Denny TP (2012) Pathogenomics of the *Ralstonia solanacearum* species complex. *Annu Rev Phytopathol* **50**: 67–89
- Gimenez-Ibanez S, Boter M, Fernandez-Barbero G, Chini A, Rathjen JP, Solano R (2014) The bacterial effector HopX1 targets JAZ transcriptional repressors to activate jasmonate signaling and promote infection in Arabidopsis. *PLoS Biol* **12**: e1001792
- Hillmer RA, Tsuda K, Rallapalli G, Asai S, Truman W, Papke MD, Sakakibara H, Jones JDG, Myers CL, Katagiri F (2017) The highly buffered Arabidopsis immune signaling network conceals the functions of its components. *PLoS Genet* **13**



- Jin H, Choi SM, Kang MJ, Yun SH, Kwon DJ, Noh YS, Noh B** (2018) Salicylic acid-induced transcriptional reprogramming by the HAC-NPR1-TGA histone acetyltransferase complex in Arabidopsis. *Nucleic Acids Res* **46**: 11712–11725
- Kim D, Landmead B, Salzberg SL** (2015) HISAT: a fast spliced aligner with low memory requirements. *Nat Methods* **12**: 357–360.
- Kunze G, Zipfel C, Robatzek S, Niehaus K, Boller T, Felix G** (2004) The N terminus of bacterial elongation factor Tu elicits innate immunity in Arabidopsis plants. *Plant Cell* **16**: 3496–3507
- Le Roux C, Huet G, Jauneau A, Camborde L, Tremousaygue D, Kraut A, Zhou B, Levaillant M, Adachi H, Yoshioka H, et al.** (2015). A receptor pair with an integrated decoy converts pathogen disabling of transcription factors to immunity. *Cell* **161**: 1074–1088
- Lewis LA, Polanski K, de Torres-Zabala M, Jayaraman S, Bowden L, Moore J, Penfold CA, Jenkins DJ, Hill C, Baxter L, et al.** (2015). Transcriptional dynamics driving MAMP-triggered immunity and pathogen effector-mediated immunosuppression in Arabidopsis leaves following infection with *Pseudomonas syringae* pv tomato DC3000. *Plant Cell* **27**: 3038–3064
- Li B, Meng X, Shan L, He P** (2016) Transcriptional regulation of pattern-triggered immunity in plants. *Cell Host Microbe* **19**: 641–650
- Li B, Jiang S, Yu X, Cheng C, Chen S, Cheng Y, Yuan JS, Jiang D, He P, Shan L** (2015) Phosphorylation of trihelix transcriptional repressor ASR3 by MAP KINASE4 negatively regulates Arabidopsis immunity. *Plant Cell* **27**: 839–856
- Liao Y, Smyth GK, Shi W** (2014) featureCounts: an efficient general purpose program for assigning sequence reads to genomic features. *Bioinformatics* **30**: 923–930
- Love MI, Huber W, Anders S** (2014) Moderated estimation of fold change and dispersion for RNA-seq data with DESeq2. *Genome Biol* **15**: 550
- Mansfield J, Genin S, Magori S, Citovsky V, Sriariyanum M, Ronald P, Dow M, Verdier V, Beer SV, Machado MA, et al.** (2012). Top 10 plant pathogenic bacteria in molecular plant pathology. *Mol Plant Pathol* **13**: 614–629
- Mukaihara T, Hatanaka T, Nakano M, Oda K** (2016) *Ralstonia solanacearum* type III effector RipAY is a glutathione-degrading enzyme that is activated by plant cytosolic thioredoxins and suppresses plant immunity. *mBio* **7**: e00359–00316
- Peeters N, Guidot A, Vailleau F, Valls M** (2013a) *Ralstonia solanacearum*, a widespread bacterial plant pathogen in the post-genomic era. *Mol Plant Pathol* **14**: 651–662
- Peeters N, Carrere S, Anisimova M, Plener L, Cazale AC, Genin S** (2013b) Repertoire, unified nomenclature and evolution of the Type III effector gene set in the *Ralstonia solanacearum* species complex. *BMC Genomics* **14**: 859
- Perez-Quintero AL, Szurek B** (2019) A decade decoded: spies and hackers in the history of TAL effectors research. *Annu Rev Phytopathol* **57**: 459–481
- Pieterse CM, Leon-Reyes A, Van der Ent S, Van Wees SC** (2009) Networking by small-molecule hormones in plant immunity. *Nat Chem Biol* **5**: 308–316
- Qi G, Chen J, Chang M, Chen H, Hall K, Korin J, Liu F, Wang D, Fu ZQ** (2018) Pandemonium breaks out: disruption of salicylic acid-mediated defense by plant pathogens. *Mol Plant* **11**: 1427–1439
- Ritchie ME, Phipson B, Wu D, Hu Y, Law CW, Shi W, Smyth GK** (2015) limma powers differential expression analyses for RNA-sequencing and microarray studies. *Nucleic Acids Res* **43**: e47
- Sarris PF, Duxbury Z, Huh SU, Ma Y, Segonzac C, Sklenar J, Derbyshire P, Cevik V, Rallapalli G, Saucet SB, et al.** (2015). A plant immune receptor detects pathogen effectors that target WRKY transcription factors. *Cell* **161**: 1089–1100
- Sato M, Tsuda K, Wang L, Collier J, Watanabe Y, Glazebrook J, Katagiri F** (2010) Network modeling reveals prevalent negative regulatory relationships between signaling sectors in Arabidopsis immune signaling. *PLoS Pathogens* **6**
- Shearer HL, Cheng YT, Wang LP, Liu JM, Boyle P, Despres C, Zhang YL, Li X, Fobert PR** (2012) Arabidopsis clade I TGA transcription factors regulate plant defenses in an NPR1-independent fashion. *Mol Plant Microbe Interact* **25**: 1459–1468
- Sun T, Busta L, Zhang Q, Ding P, Jetter R, Zhang Y** (2018) TGACG-BINDING FACTOR 1 (TGA1) and TGA4 regulate salicylic acid and piperolic acid biosynthesis by modulating the expression of SYSTEMIC ACQUIRED RESISTANCE DEFICIENT 1 (SARD1) and CALMODULIN-BINDING PROTEIN 60g (CBP60g). *New Phytol* **217**: 344–354
- Tateda C, Zhang ZQ, Shrestha J, Jelenska J, Chinchilla D, Greenberg JT** (2014) Salicylic acid regulates Arabidopsis microbial pattern receptor kinase levels and signaling. *Plant Cell* **26**: 4171–4187
- Wang W, Withers J, Li H, Zwack PJ, Rusnac DV, Shi H, Liu L, Yan S, Hinds TR, Guttman M, et al.** (2020). Structural basis of salicylic acid perception by Arabidopsis NPR proteins. *Nature* **586**: 311–316
- Wei Y, Caceres-Moreno C, Jimenez-Gongora T, Wang K, Sang Y, Lozano-Duran R, Macho AP** (2018) The *Ralstonia solanacearum* csp22 peptide, but not flagellin-derived peptides, is perceived by plants from the Solanaceae family. *Plant Biotechnol J* **16**: 1349–1362
- Wei Y, Balaceanu A, Rufian JS, Segonzac C, Zhao A, Morcillo R, Macho AP** (2020) An immune receptor complex evolved in soybean to perceive a polymorphic bacterial flagellin. *Nat Commun* **11**: 3763
- Wu D, von Roepenack-Lahaye E, Buntru M, de Lange O, Schandry N, Perez-Quintero AL, Weinberg Z, Lowe-Power TM, Szurek B, Michael AJ, et al.** (2019). A plant pathogen type III effector protein subverts translational regulation to boost host polyamine levels. *Cell Host Microbe* **26**: 638–649.e5
- Xian L, Yu G, Wei Y, Rufian JS, Li Y, Zhuang H, Xue H, Morcillo R, Macho AP** (2020) A bacterial effector protein hijacks plant metabolism to support pathogen nutrition. *Cell Host Microbe* **28**: 548–557
- Xu J, Xie J, Yan CF, Zou XQ, Ren DT, Zhang SQ** (2014) A chemical genetic approach demonstrates that MPK3/MPK6 activation and NADPH oxidase-mediated oxidative burst are two independent signaling events in plant immunity. *Plant J* **77**: 222–234
- Yu X, Feng BM, He P, Shan LB** (2017) From chaos to harmony: responses and signaling upon microbial pattern recognition. *Annu Rev Phytopathol* **55**: 109–137
- Zhang Y, Li X** (2019) Salicylic acid: biosynthesis, perception, and contributions to plant immunity. *Current Opin Plant Biol* **50**: 29–36
- Zhang YL, Tessaro MJ, Lassner M, Li X** (2003) Knockout analysis of Arabidopsis transcription factors TGA2, TGA5, and TGA6 reveals their redundant and essential roles in systemic acquired resistance. *Plant Cell* **15**: 2647–2653
- Zhang YL, Fan WH, Kinkema M, Li X, Dong XN** (1999) Interaction of NPR1 with basic leucine zipper protein transcription factors that bind sequences required for salicylic acid induction of the PR-1 gene. *Proc Natl Acad Sci USA* **96**: 6523–6528
- Zheng XA, Li XJ, Wang BS, Cheng D, Li YP, Li WH, Huang MS, Tan XD, Zhao GZ, Song BT, et al.** (2019). A systematic screen of conserved *Ralstonia solanacearum* effectors reveals the role of RipAB, a nuclear-localized effector that suppresses immune responses in potato. *Mol Plant Pathol* **20**: 547–561
- Zheng XY, Spivey NW, Zeng WQ, Liu PP, Fu ZQ, Klessig DF, He SY, Dong XN** (2012) Coronatine promotes *Pseudomonas syringae* virulence in plants by activating a signaling cascade that inhibits salicylic acid accumulation. *Cell Host Microbe* **11**: 587–596
- Zhou JM, Zhang Y** (2020) Plant immunity: danger perception and signaling. *Cell* **181**: 978–989
- Zhou JM, Trifa Y, Silva H, Pontier D, Lam E, Shah J, Klessig DF** (2000) NPR1 differentially interacts with members of the TGA/OBF family of transcription factors that bind an element of the PR-1 gene required for induction by salicylic acid. *Mol Plant Microbe Interact* **13**: 191–202